Spring 2019

Numerical Analysis on Convective Cooling Augmented by Evaporative Heat and Mass Transfer for Thermal Power Plant Application

Sudipta Saha

NUMERICAL ANALYSIS ON CONVECTIVE COOLING AUGMENTED BY EVAPORATIVE HEAT AND MASS TRANSFER FOR THERMAL POWER PLANT APPLICATION

by

Sudipta Saha

Bachelor of Science
Bangladesh University of Engineering and Technology, 2013

Submitted in Partial Fulfillment of the Requirements

For the Degree of Master of Science in

Mechanical Engineering

College of Engineering and Computing

University of South Carolina

2019

Accepted by:

Tanvir Farouk, Director of Thesis

Jamil Khan, Reader

Cheryl L. Addy, Vice Provost and Dean of the Graduate School

DEDICATION

The author dedicates this work to the selfless and altruistic human rights activists and social reformers who work relentlessly to make this world a better place.

.

ACKNOWLEDGEMENTS

I wish to express my deepest gratitude and appreciation to my advisor, Dr Tanvir Farouk, for his guidance and encouragement throughout. I thank him for giving me the opportunity to work under his supervision in my concurrent MS and PhD program.

I am grateful to Dr Jamil Khan, Chair of my department, and Dr Fahd Ebna Alam, my former lab mate, who encouraged me to attain MS degree through my journey towards doctoral degree. With their selfless advice, I decided to utilize my work on heat and mass transfer as a thesis work for my MS degree.

I like to thank Dr Tamanna Alam and Dr Tital Paul, who always welcomed me when I sought advices on academic endeavor. I am grateful to my fellow lab mates, Ali Charchi Aghdam, Sheikh Farhan Ahmed and Malik M Tahiyat for their continuous support and cooperation.

I like to express my deepest gratitude to my family members. My father, Dr Subas Chandra Saha, has always been an inspiration to me. My mother, Chandana Saha, sacrificed throughout her life for the sake of my success. My younger brother, Auritra Saha has always been a great support for me in all situations. Finally, a very special thanks to my wife, Anu Pria Roy for her caring and supportive presence in my family and work life.

.

ABSTRACT

This thesis work describes a numerical study on the effect of evaporative cooling on the augmentation of forced convective cooling. In recent years, on-demand phase change boosted cooling has drawn major interest where convective heat transfer is augmented/aided by evaporative heat and mass transport processes. This dual mode (convection and evaporation) cooling method is envisioned to drastically enhance the heat transfer coefficient where conventional convective cooling has already reached its maximum value and furthermore dry cooling is still a desired objective. A multi-dimensional mathematical model has been developed to conduct simulations over a range of operating parameters to obtain insight into the 'hybrid' system where phase change process and convection both contribute to the heat transfer process. The system being modeled consists of a thin liquid water film that undergoes evaporation as a result of being exposed to a prescribed heat flux and laminar convective flow condition. The mathematical model utilized comprises of coupled conservation equations of mass, species, momentum and energy for the convection-evaporation domain (gaseous), and only mass and energy conservation being resolved in the liquid film domain, together with a moving mesh to resolve the receding liquid film. Predictions from the simulations indicate that in comparison to pure forced convection cooling, under convective-evaporative conditions the overall heat transfer coefficient is increased by a factor of ~ 5, where evaporation alone contributes to 80% - 90% of the overall performance. For a fixed heat flux, an increase in Reynolds number was found to increase the heat transfer

coefficient and vice versa for film thickness. It has been found that overall heat transfer coefficient can be enhanced by making the film thinner, since the conducting resistance across the liquid film diminishes as the film thickness is reduced. A critical film thickness has been identified beyond which the conductive resistance becomes dominant and starts to attenuate the thermal performance. Spatiotemporally averaged interface temperature has been found to be increasing with the increase of film thickness, as an evidence of suppressed cooling. A critical Reynolds number is identified beyond which no significant increase in overall heat transfer coefficient is observed. Furthermore, surface enhancement studies have been conducted with view to assessing its effect on overall thermal performance of convective-evaporative dual mode heat transfer system. To accomplish that, bottom surface of the evaporating liquid has been modified by introducing circular grooves to promote mixing. A set of parametric study based on enhanced surface structures predicts that surface modification results in a significant reduction in thermal resistance across the liquid film.

TABLE OF CONTENTS

LIST OF TABLES

LIST OF FIGURES

LIST OF ABBREVIATIONS

ACC .....Air Cooled Condenser

FCC ..... Forced Convective Cooling

HTC..... Heat Transfer Coefficient

SBC .....Sweating Boosted Cooling

WCC ..... Water Cooled Condenser

CHAPTER 1

INTRODUCTION

1.1. PROBLEM STATEMENT

Phase change heat transfer has been a major topic of research due to its robustness over sensible heat transfer in practical application. The cooling process determines the efficiency in many applications such as thermal powerplants. An effective heat transfer module aided by phase change heat transfer can significantly improve the overall performance of a thermal powerplant. Water cooled condensers (WCC) are widely used for cooling purpose in thermal power plants as well as in other industrial applications. It

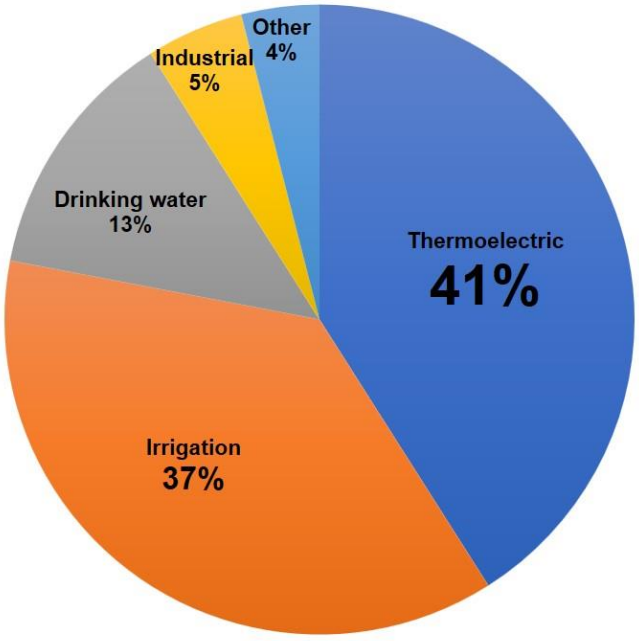

Figure 1.1: Share of fresh water withdrawals from major applications in U.S. in 2005 [1]

has been reported that approximately 100,000 millions of gallons of water was used per day for such cooling processes in 2015 in USA [2]. Thermal powerplants account for 41% of the total freshwater used in the United States [1, 3]. The fresh water withdrawal in different processes in the United States has been illustrated in Figure 1.1 and 1.2. The US federal government currently aims for a reduction of annual water usage by ~2% [4] to move forward towards a greener economy. This drives the need to find an effective dry cooling strategy as an alternative to WCC. Air cooled condenser (ACC) have great potential to be considered as an immediate replacement as it reduces water consumption

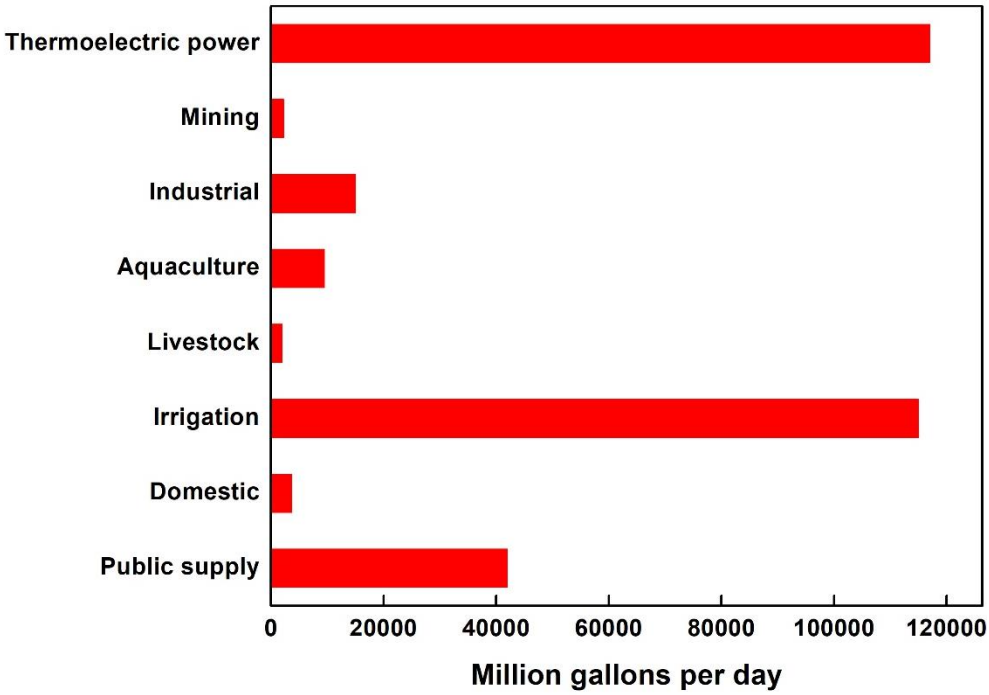

Figure 1.2: Water usage in different application in U.S. in 2015 [2]

to a large degree. However, it does have several drawbacks [5]. To compensate the low heat transfer performance of air, to meet the same targets an ACC design needs to be significantly larger in size which leads to an appreciable increase in the production and

capital cost. For a same working fluid, the forced convective cooling can be enhanced by increasing the convective velocity and alternately modifying the surface structures [6-8] and materials [9, 10]. Several methods have been demonstrated and employed, including nanomaterials [11, 12], porous media [13-15], micro-channels [16-18] and spray cooling arrangements [19, 20] all of which had the target objective of attaining a higher heat transfer coefficient. However, most of these novel methods suffer from scale up for large application (e.g. thermal power plants) due to the associated high expenses.

For large scale applications, it has been a challenge to identify a possible and effective methodology/process that minimizes the trade-off between WCC and ACC. A suitable alternative to WCC, which reduces water consumption significantly and can also overcome the limitations of ACC, is therefore a research topic that is of immense interest. A possible way of addressing this challenge is to introduce phase change phenomena inspired by the natural perspiration process (i.e. sweating) of mammals that would augment the force convective cooling and enhance the overall cooling performance. This on demand sweating boosted cooling is envisioned to drastically reduce water usage [21-23]. Evaporation, being one of the ubiquitous processes in nature, still requires extensive studies to fully understand the physics and thermodynamics associated with it. The system gets even more complex when fluid flow and external heat transfer come into play. Therefore, there is a need to understand the fundamentals of this mixed mode heat transfer system experiencing both convective and evaporative heat and mass transfer. This work is dedicated to exploring the key features and obtain insights on this proposed dual mode heat transfer with a view to having higher heat transfer coefficient.

1.2. LITERATURE REVIEW

Simultaneous heat and mass transport under convective environment has been a topic of interest [24-27] with a view to understand the fundamentals of the coupled dynamic system. The early work of Vyazovov [28] led to the development of a simplified model for isothermal absorption in a falling liquid film; a representative of combined mass and heat transfer system. With a similar approach, Olbrich and Wild [29] solved species diffusion equation in laminar flow condition for several falling film geometries. Both these studies dealt with mass transfer only, where the effect of heat transfer was not taken into account, hence the coupling between the heat and mass transport was neglected. A theoretical analysis of mixed mode heat and mass transfer in the absorption of water vapor into a laminar liquid film was conducted by Grossmann [30]. Temperature and concentration variation were analyzed for an imposed parabolic velocity profile by solving coupled energy and species diffusion equation mathematical model. Numerical simulations were conducted by Yih and Seagrave [31] to study mass transport driven by heat transfer when exposed to a uniform velocity profile under laminar conditions.

As an attempt to improve the prior models, Yan et al. [32] proposed a mathematical model that had a strong coupling among momentum, species and energy equations and the model was employed to simulate the combined heat and mass transfer between a vertical parallel plate under laminar flow condition. A similar study was conducted by Whitaker [33] for a porous media configuration. In all these studies a liquid film of constant and non-evolving thickness was considered. The dependence of film size on laminar and turbulent convection was investigated by Yan [24, 25] and it was

identified that film thickness does play a significant role on the net mass transfer across the phases. This highlights that in the context of thin film evaporation, the temporal evolution (i.e., recession) of film thickness may play a critical role in the physical process. Chow and Chung [34] investigated evaporation of water into a laminar stream of dry air, humid air and superheated steam from a large reservoir. Studies on mixed convection heat and mass transfer in a vertical channel with film evaporation have also been reported by Cherif et al. [35]. In both these studies a prescribed mass concentration of liquid vapor was provided at the interface and the evaporation flux was calculated afterwards. The mass concentration was estimated from equation of state assuming ideal air-vapor mixture and saturation condition at the interface. A careful reexamination of these major studies shows that further investigation is needed to unravel the evaporation assisted convective heat transfer system to assess its promise in defeating the trade-off between air-cooled and water-cooled condenser.

1.3. SCOPE AND ORGANIZATION OF THIS THESIS WORK

This sweating boosted cooling configuration, inspired by the natural perspiration process of mammals, has the potential to drastically reduce water consumption and enhance the heat transfer effect simultaneously. A schematic of power generation plant with proposed sweating boosted air-cooled condenser is presented in Figure 1.3. In this arrangement, water introduced as drips in the exterior of the air-cooled condenser undergoes evaporation and augments the cooling process.

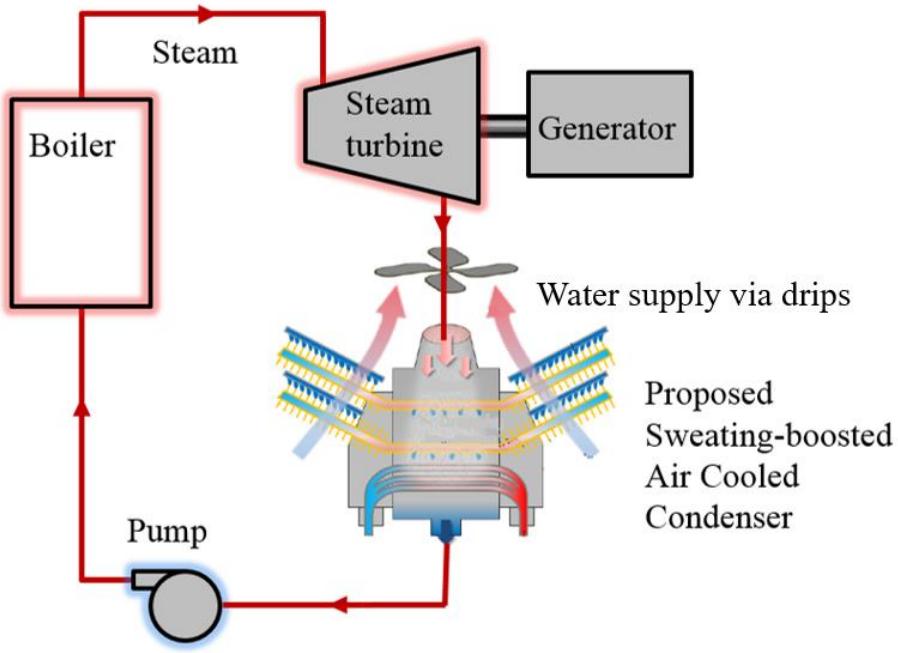

Figure 1.3: Schematic of a power generation plant with the proposed sweating-boosted air-cooled condenser

Main objective of this study is to numerically assess the performance of the proposed sweating boosted cooling method in defeating the trade-off between air-cooled and water-cooled condenser. In order to accomplish this, improvement upon the previous efforts on modeling combined heat and mass transfer under convective environment has been attained to simulate convective heat transfer augmented by phase change process. The proposed model solves a strongly coupled mass, momentum, and energy conservation equations together with individual species transport for a multiphase convective environment configuration. The depletion of the liquid phase is also resolved to predict the highly transient characteristics of evaporation which is a key element of on-demand evaporation/sweating boosted convective heat transfer. Predictions from the model provide insight on the role of the key parameters on the overall heat transfer process.

Following the problem description, background study and objectives presented in Chapter 1, next three chapters are organized based on illustration of the model development process. Chapter 2 depicts the schematic of problem geometry along with the physical parameters utilized in the simulation. The mathematical model development with appropriate boundary conditions has been articulated in Chapter 3. Chapter 4 presents detailed description on numerical methods employed in this study. Mesh/grid dependency analysis has also been presented in this chapter.

Chapter 5 contains the results predicted by the numerical model for a broad range of parametric conditions along with analytical and experimental validation. The advantage of the proposed sweating-boosted cooling to find a trade-off between air-cooled condenser and water-cooled condenser has been discussed by comparing the global feature of heat exchangers i.e., area footprint and water consumption. Finally, Chapter 6 serves as a closure of this thesis work summarizing the contribution of the author in the field of study. Chapter 6 culminates with the major findings of this study and recommendation for future research direction.

.

CHAPTER 2

COMPUTATIONAL DOMAIN AND PHYSICAL PARAMTERS

2.1. SCHEMATIC OF PROBLEM GEOMETRY

A schematic diagram of the system that is being simulated in presented in Figure 2.1. The phase change augmented cooling system comprises of a thin evaporating liquid water film which is exposed to a laminar air flow.

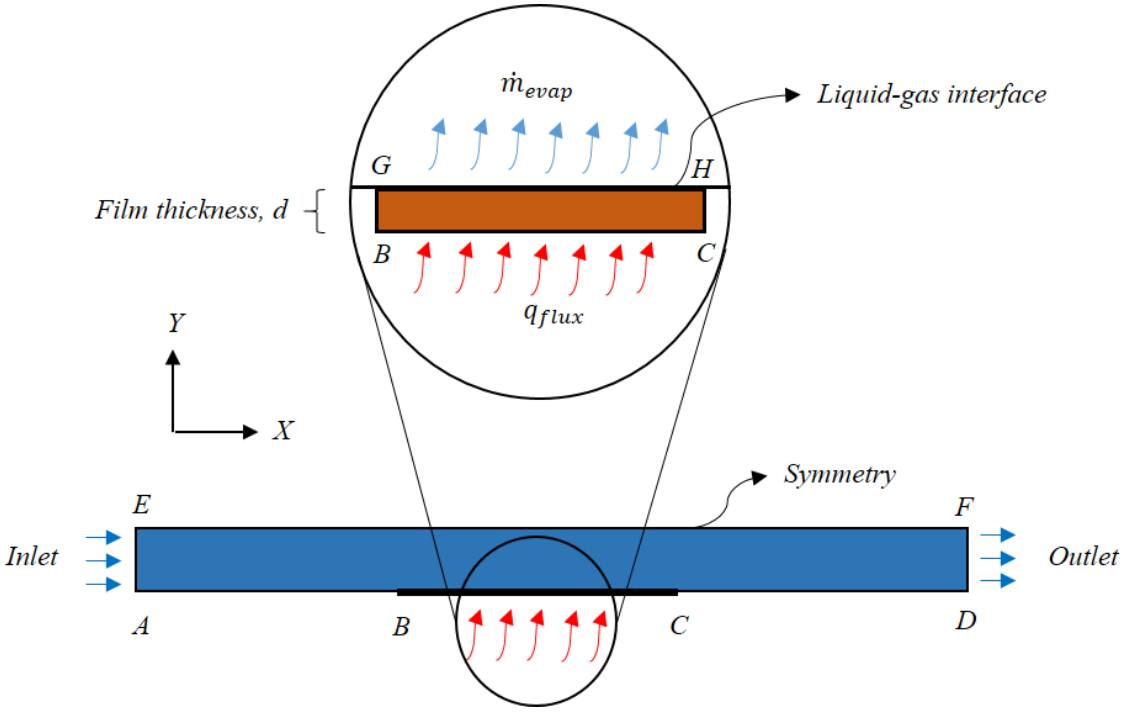

Figure 2.1: Schematic of the problem geometry and computational domain (not it scale)

The two-dimensional domain comprises of gas domain (ADFE) and a thin evaporating liquid domain (BCHG). The film is prescribed in a depressed cavity which is consistent to the experiments conducted by Wang et al.[21, 22]. The film is exposed to a

laminar air flow and a constant heat flux (q_{flux}) is prescribed at the bottom of the film. Initial film thickness (BG) and the film width (GH) is prescribed that dictates the water load. During the course of evaporation, the liquid domain (BCHG) diminishes as water is being evaporated and carried away by the incoming air. The liquid-gas interface (GH) thus recedes downward gradually as the water is being depleted.

2.2. PHYSICAL PARAMETERS

The parameters that were varied in the simulations are the free stream velocity and liquid film thickness. A list of the different parameters considered in the simulations and associated geometric dimensions are summarized in Table 2.1.

Table 2-1: Parameters for sweating-boosted cooling simulations

Physical Parameter	
Velocity (U_∞)	1 – 30 m/s
Film thickness (d)	5 – 1000 μm
Heat flux (q_{flux})	1256 W/m^2
Ambient temperature, (T_∞)	300 K

Geometric Entity	
AB	5.0 (cm)
BC	5.0 (cm)
CD	5.0 (cm)
AE	0.5 (cm)
BG	d

CHAPTER 3

MATHEMATICAL MODELING

3.1. GAS PHASE CONSERVATION EQUATION

In the gas phase conservation of averaged mass, momentum and energy is considered together with a species conservation equation for the water vapor to resolve the transport of water vapor in the gas domain resulting from the evaporation process. The conservation equations have the following form:

$$\frac{\partial}{\partial t}(\rho_{mix,g}) + \nabla.(\rho_{mix,g}\bar{u}) = 0 \tag{1}$$

$$\frac{\partial}{\partial t}(\rho_{mix}\bar{u}) + \nabla.(\rho_{mix}\bar{u}\bar{u}) = -\nabla p + \nabla.\tau \tag{2}$$

$$\frac{\partial}{\partial t}(\rho_{mix}C_{p,g}T) + \nabla.(\rho_{mix}C_{p,g}\bar{u}T) = -\nabla.q \tag{3}$$

$$\frac{\partial}{\partial t}(\rho_{mix}Y_k) + \nabla.(\rho_{mix}\bar{u}Y_k) = -\nabla.(\rho_{mix}D_k\nabla Y_k) \tag{4}$$

where, $\rho_{mix,g}$ is the mixture density , τ is the shear stress tensor, $\bar{u}$ is the velocity vector, p is the pressure, $C_{p,g}$ is the specific heat capacity of the gas mixture, Y_k and D_k is the mass fraction and mass diffusivity of water vapor in air respectfully.

3.2. LIQUID PHASE CONSERVATION EQUATION

In the liquid phase, only the energy conservation equation is solved assuming that the heat transfer across the liquid film is due to conduction only. The energy conservation equation in the liquid phase has the following expression:

$$\frac{\partial}{\partial t}\left(\rho_l C_{p,l} T\right) = \nabla.\left(k_l \nabla T\right) \tag{5}$$

where, ρ_l, $C_{p,l}$ and k_l is the density, specific heat capacity and conductivity of liquid water respectively.

3.3. BOUNDARY CONDITIONS

At the interface (GH), a modified Hertz-Knudsen (HK) relation [36, 37] is employed to express the evaporative mass flux and resulting net mass transfer at the liquid-gas interface. The modified HK relation assumes the accommodation coefficient associated with evaporation and condensation to be similar ($\sigma_e = \sigma_c$) and an identical liquid and vapor phase temperature at the interface ($T_l = T_v$) [38-41]. The evaporative mass flux at the liquid-vapor interface resulting from the modified HK relationship has the following expression [36, 37]:

$$j_{evap} = \sigma \sqrt{\frac{M}{2\pi R T_l}} \left[\left(P_s\left(T_l\right) - P_v\right)\right] \tag{6}$$

where, j_{evap} is the evaporative mass flux, M is the molecular weight, R is the universal gas constant, P_s is the saturation pressure, P_v is the partial vapor pressure. T_l is liquid temperature at the interface and σ is the accommodation coefficient.

The partial vapor pressure P_v is determined from the mass fraction of the water vapor present in the air-water vapor mixture in the gas domain which is found from the solution of the gas phase species conservation equation. Antoine equation [42] is used to calculate the saturation pressure which has the following expression:

$$log\left(P_s\right) = A - \frac{B}{T_l} \tag{7}$$

where, A=20.386 and B = 5132 for water for a temperature range of 1 – 99^{o}C.

At the liquid-gas interface (GH) which experiences the evaporative mass transfer a normal velocity is prescribed which is obtained from the evaporative mass flux, $\bar{n}.\bar{u} = \frac{j_{evap}}{\rho_v}$ where, $\bar{n}$ is the unit outward vector normal to the interface and ρ_v is the density of the water vapor.

For the species conservation equation, a flux balance for the water vapor is prescribed at the interface:

$$\bar{n}.j_{evap} = \rho_{mix} D_k \nabla Y_k - \rho_{mix} \bar{u} Y_k \tag{8}$$

The net evaporation rate is obtained from the evaporation flux and the interface surface area:

$$\dot{m}_{evap} = j_{evap} A_s \tag{9}$$

where, A_s is the free surface area of the liquid film exposed to the ambient.

An energy balance condition is provided at the interface where the energy flux in the liquid phase is balanced by the energy flux in the gas phase and the heat loss associated with the latent heat of evaporation:

$$q_l - q_g = q_{evap} \tag{10}$$

where, q_l is the heat flux in the liquid phase having contribution from conduction alone, q_g is the heat flux in the gas phase having contribution from both conductive and convective fluxes and q_{evap} is the evaporative heat loss determined from the evaporative flux and latent heat of vaporization ($q_{evap} = \dot{m}_{evap} h_{fg}$)

Since the liquid film recedes with time as result of the evaporative process, changing the spatial position of liquid-vapor interface, a moving mesh technique is implemented to track the change in the spatial location of the liquid-vapor interface. An

Arbitrary Lagrangian-Eulerian (ALE) [43] technique with a Laplace smoothing approach is employed for this purpose. In the ALE method, the following equations are solved:

$$\frac{\partial^2}{\partial X^2}\frac{\partial x}{\partial t}+\frac{\partial^2}{\partial Y^2}\frac{\partial x}{\partial t}=0 \tag{11}$$

$$\frac{\partial^2}{\partial X^2}\frac{\partial y}{\partial t}+\frac{\partial^2}{\partial Y^2}\frac{\partial y}{\partial t}=0 \tag{12}$$

where, X and Y are the material frame coordinates and x and y are the mesh coordinates. Since the dissipation is occurring only in the y direction, the mesh displacement along the x direction is considered to be negligible. Mesh displacement along the y direction at time t is calculated by, $\Delta y = v_{mesh} t$, where, v_{mesh} is the moving mesh velocity that is obtained from the evaporative mass flux expression, $v_{mesh} = j_{evap} / \rho_l$ Details on the additional boundary conditions employed are summarized in Table 3.1. The notations in the table correspond to the schematic diagram presented in Figure 2.1.

Table 3-1: Boundary conditions in the gas and liquid phase

Phases	Boundary	Prescribed Boundary Condition
Gas (air-water vapor mixture)	AE (Inlet)	$u = U_\infty, v = 0$ $T = T_\infty$ $Y_k = 0, Y_{air} = 1$
	DF (Outlet)	$-\bar{n}.\nabla\bar{u} = 0$ $-\bar{n}.\nabla T = 0$ $-\bar{n}.\nabla Y_k = 0$
	EF (Symmetry)	$\bar{u}.\bar{n} = 0, -\bar{n}.\nabla\bar{u} = 0$ $-\bar{n}.\nabla T = 0$ $-\bar{n}.\nabla Y_k = 0$
	AG, HD (no slip, thermal insulation, no	$\bar{u} = 0$ $-\bar{n}.\nabla T = 0$ $-\bar{n}.\nabla Y_k = 0$

	flux)	
Liquid (water film)	BC	$-\bar{n}.\left(-k_l \nabla T\right) = q_{flux}$
	BG, CH (thermal insulation)	$-\bar{n}.\nabla T = 0$

CHAPTER 4

NUMERICAL METHODS

4.1. NUMERICAL SCHEMES

The system of equations is discretized on the basis of finite element method and is solved using a time-dependent solver in COMSOL Multiphysics® software [44]. The computational domain is meshed using a non-uniform distribution of structured quadrilateral elements, having higher mesh density at and along the non-slip boundary surface to accurately resolve the velocity and thermal boundary layer. A total number of 15,500 quadrilateral elements are used with a maximum and minimum grid size of 180 μm and 1 μm respectively. The time integration was performed using a fully implicit backward difference (BDF) scheme with variable time stepping having a minimum and maximum time step of 1.0×10^{-6} and 0.2 seconds. The numerical solution of the coupled sets of equation was obtained using the **Mu**ltifrontal **M**assively **P**arallel **S**parse (MUMPS) direct solver [45].

4.2. GRID INDEPENDENCE

The mesh sizes used for the analyses are chosen as such to ensure grid independent solutions. Figure 4. presents the quasi-steady temperature of the bottom wall of the depressed cavity (BC) and overall heat transfer coefficient as a function of total grid numbers. The overall heat transfer coefficient is obtained from the energy balance of

the coupled convective-evaporative process; $q_{flux} = h_{SBC}\left(\bar{T}_{int} - T_{\infty}\right)$ where, q_{flux} is the input heat flux, h_{SBC} is the overall heat transfer coefficient of convective-evaporative cooling

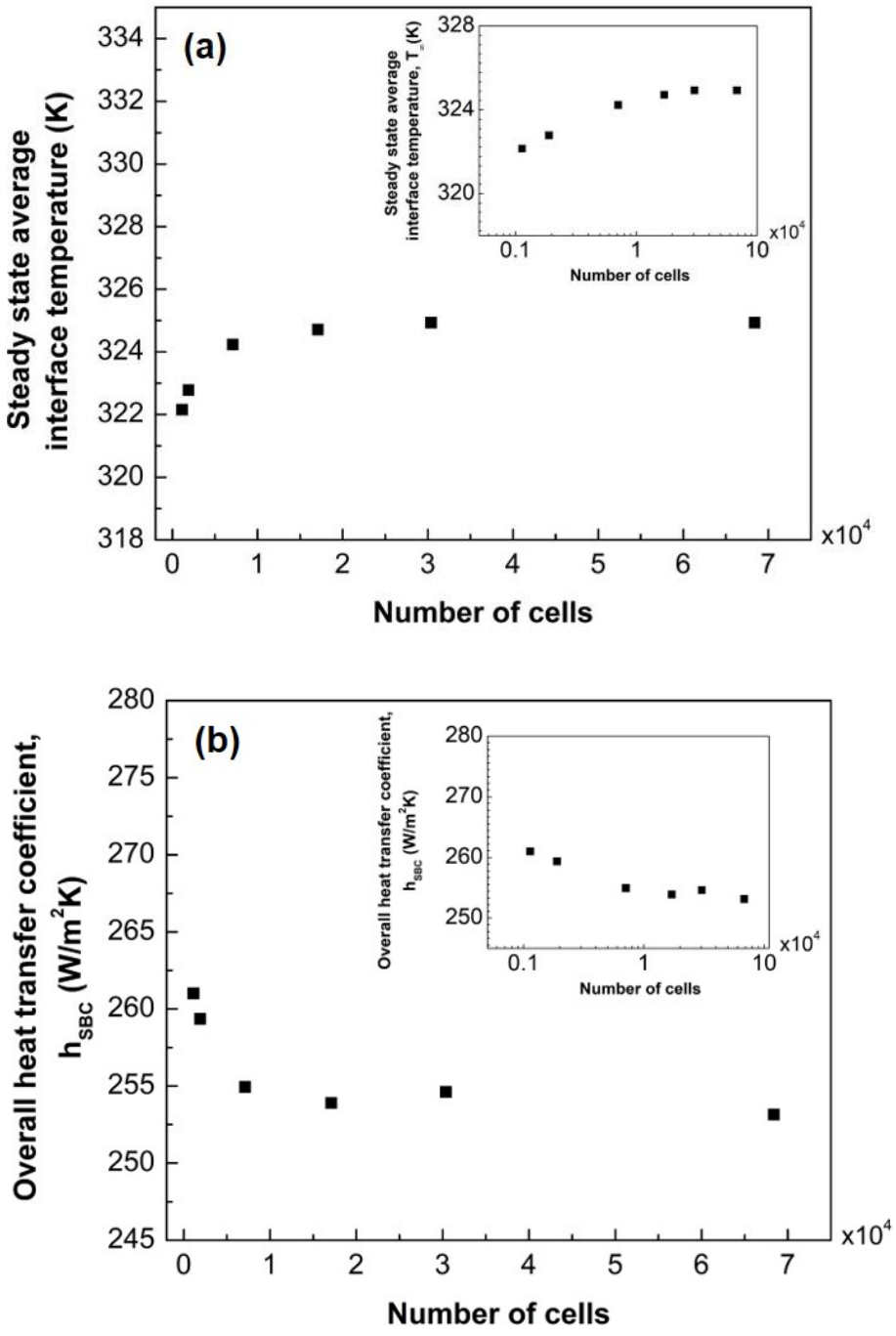

Figure 4.1: Grid size dependence study on (a) steady state average interface temperature and (b) over all heat transfer coefficient (q_{flux} = 1256 W/m^2, d = 50 μm, σ = 0.0001)

and $\bar{T}_{int}$ is the spatially averaged interface temperature during convection-evaporation period and simply wall temperature during the convective period when the liquid film is completely depleted, and the depressed cavity is empty. It is evident that for a total grid number that is greater than 15,000 a grid independent solution is achieved.

Simulations were conducted for multiple cycles of convective-evaporative transport where a prescribed liquid film is completely consumed and is reintroduced again. A single convective-evaporative cycle is complete when a prescribed liquid film is completely evaporated and the system further undergoes convective cooling only for a prescribed time. The multi-cycle simulations were conducted by providing the final spatiotemporal solution of a convective-evaporative cycle as the initial condition. In a new cycle the water film is reintroduced and the evaporation process starts taking place consequently.

CHAPTER 5

RESULTS AND DISCUSSION

5.1. ANALYTICAL VALIDATION

The simulation results are first compared against analytical solution for validation purpose. The geometric configuration of this study is analogous to forced convection over a flat plate having an unheated starting length showed in Figure 5.1

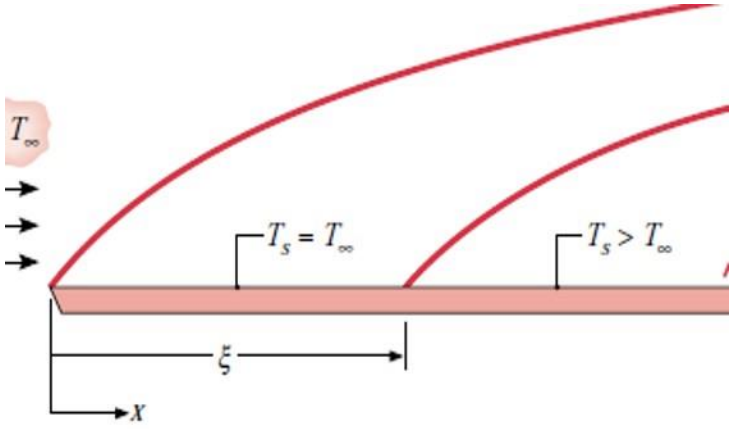

Figure 5.1: Schematic diagram of forced convection over flat plate having unheated starting length [46]

The average Nusselt number ($\overline{Nu_L}$) for a flat plate with constant heat flux can be expressed by the analytical expression, $\overline{Nu_L} = 0.68 Re_L^{1/2} Pr^{1/3}$ [46], which takes the following form when an unheated starting length is considered,

$\overline{Nu_L} = \overline{Nu}_{\zeta=0} \frac{L}{L-\zeta}\left[1-\left(\frac{\zeta}{L}\right)^{\frac{Z+1}{Z+2}}\right]^{\frac{Z}{Z+1}}$. In this expression ζ is the unheated starting length and Z is a constant coefficient that denote laminar or turbulent flow conditions. For a laminar flow, $Z = 2$.

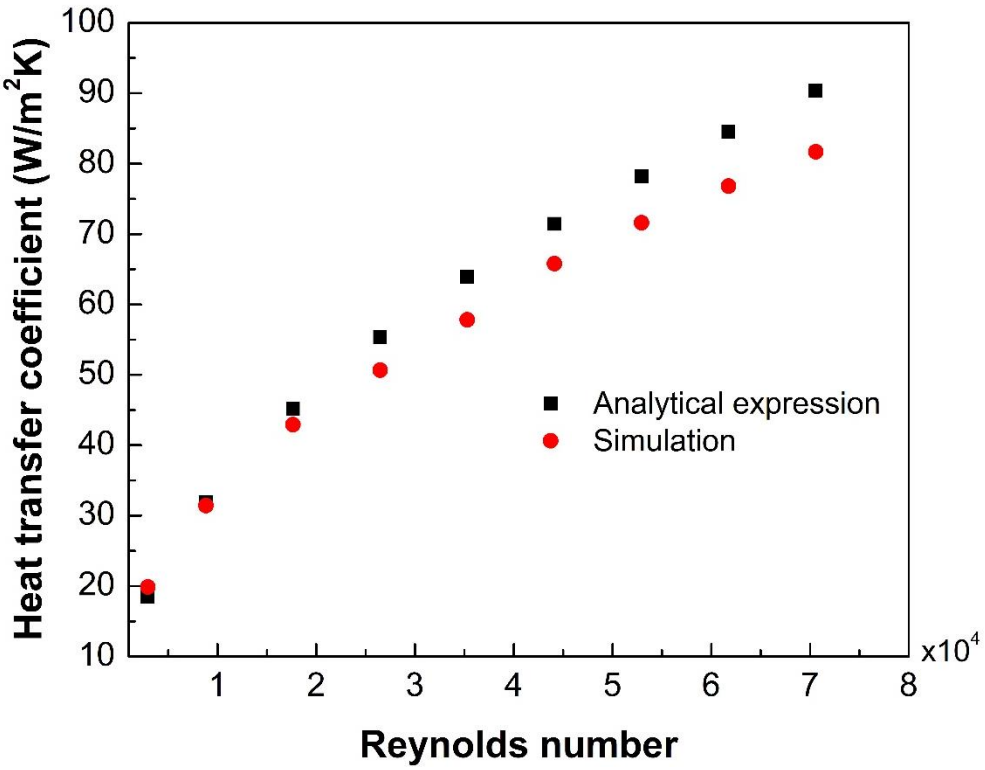

Figure 5.2: Comparison between numerically and analytically obtained heat transfer coefficient for a flat plate with unheated starting length (q_{flux} = 1256 W/m^2, d = 50 μm)

Figure 5.2 compares the numerically predicted heat transfer coefficient against the one obtained from the aforementioned analytical expression. This comparison is drawn for a purely convective mode of operation only. It is observed that at lower Reynolds number the numerical predictions and the analytical values are almost identical. However, at higher Reynolds numbers, a slight deviation between them is observed. At

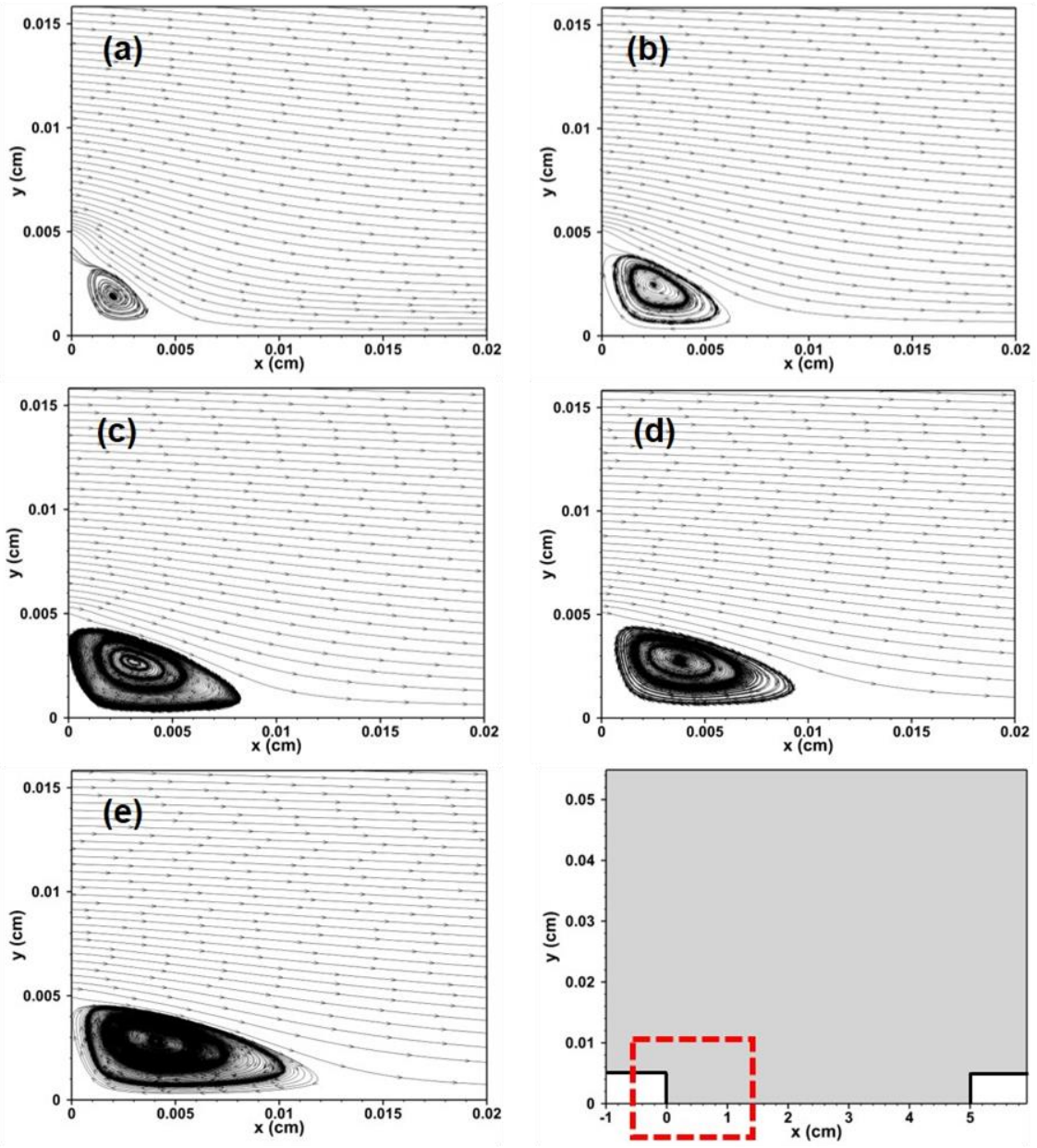

Figure 5.3: Streamline patterns near the leading edge of the recessed cavity (BCHG in Figure 2) for different Reynolds number (a) Re = 8370, (b) 26007, (c) Re = 43944, (d) Re = 61921, and (e) Re = 70948 (q_{flux} = 1256 W/m^2, d = 50 μm). The location of the recirculation zone in respect to the depressed cavity is shown with the dashed box.

higher Reynolds number the maximum variation between the numerical and analytical values was found to be ~10 W/m^2 K. A possible reason for this variation could be due to the fact that, the analytical relation holds true strictly for a flow over a flat plate whereas

the geometric configuration for the current study has a rectangular region that is slightly recessed (at x = B in Figure 2.1). As the Reynolds number increases, localized recirculation zones are formed near the leading and trailing edge of the depressed cavity. At higher Reynolds numbers, the extent of the recirculation zone increases (Figure 5.3) which impacts the overall heat transfer process.

5.2. TEMPORAL ANALYSIS OF SWEATING-BOOSTED COOLING SYSTEM

The proposed sweating boosted cooling combines the dual effect of convection and evaporation; it is a convective cooling process accompanied by phase change heat and mass transfer. The process is highly transient and alternates between a dual convective-evaporative mode to a pure convective mode. Figure 5.4 presents a temporal evolution of the average evaporation flux and the liquid-gas interface temperature for the base case (U_∞ = 9 m/s/Re = 26007, q_{flux}= 1256 W/m^2, d = 50 μm, σ = 0.0001) for multiple cycles. The average evaporation flux and interface temperature is obtained by performing a spatial average along the entire liquid-gas interface. The transient characteristics of the system is evident as both the evaporation flux and the corresponding interface temperature represent a temporally evolving cyclic profile. Figure 5.4 further shows that each cycle consists of two modes of operations - sweating-boosted cooling (SBC) resulting from the evaporative process and pure forced convective cooling (FCC). At the very initial stage the system is subjected to a very high evaporation flux (~ 1.2 g/m^{2}s). This is due to the fact that during the initial stage, the local temperature is significantly elevated as a result of the assigned heat flux and at the same time a larger difference between the saturation pressure and the partial pressure of the liquid vapor exists. Due to this high evaporation flux at the initial stage, the liquid-vapor interface temperature tends

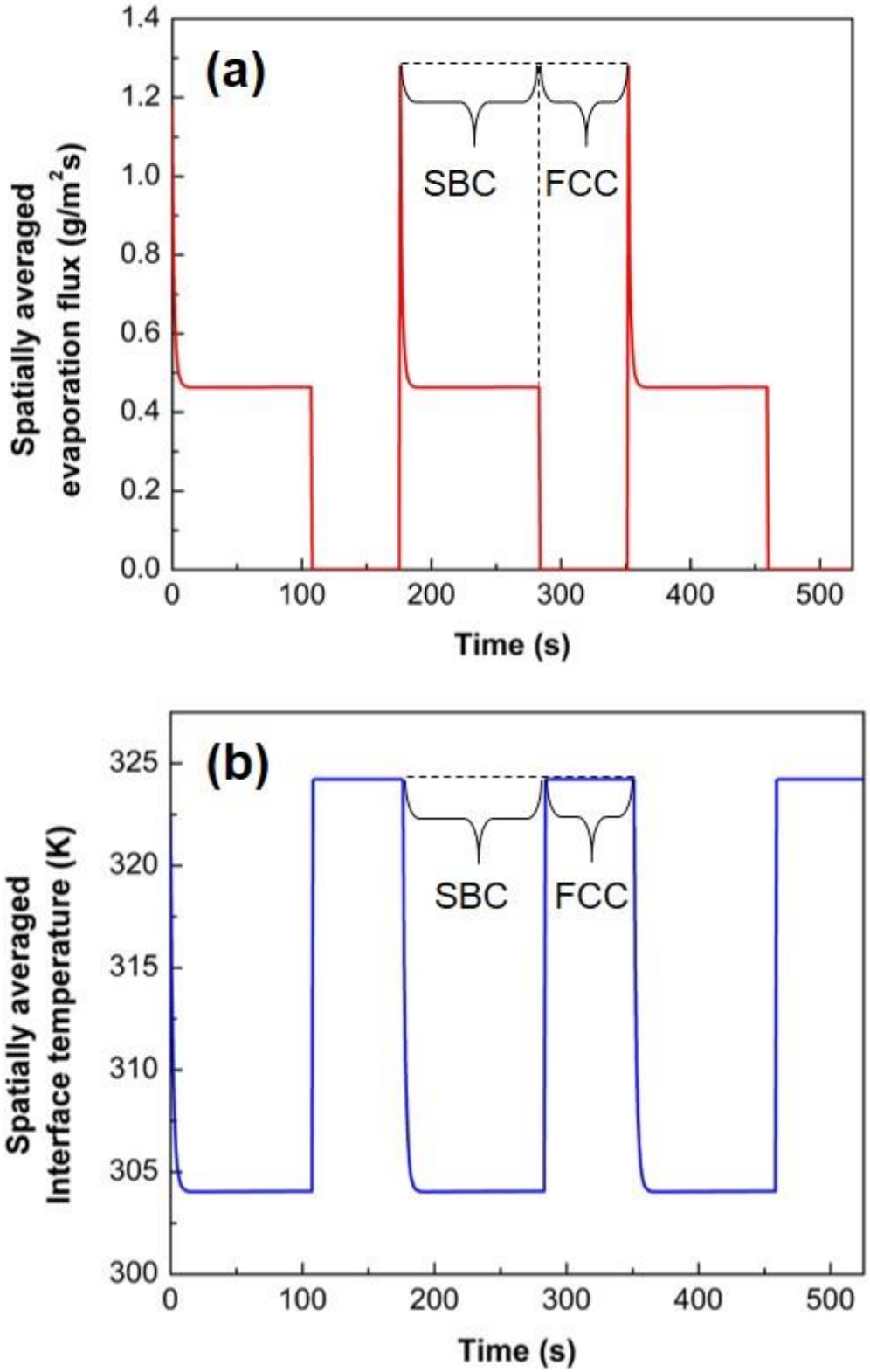

Figure 5.4: Temporal evolution of the spatially averaged (a) evaporation flux and (b) interface temperature for the base case (U_∞ = 9 m/s/Re = 26007, q_{flux} = 1256 W/m^2, d = 50 μm, σ = 0.0001). Temporal locations of sweating-boosted cooling (SBC) and forced convection cooling (FCC) are also demarcated

to decrease sharply as a consequence of the latent heat of vaporization and reaches a quasi-steady temperature of ~304 K. Consequently, the evaporation rate decreases and attains a quasi-steady rate of ~ 0.45 g/m^{2}s due to the strong dependency of the evaporation flux on the local temperature. It can be seen that the quasi-steady evaporation rate and interface temperature overlap with each other denoting that the quasi-steady cooling is achieved predominantly due to the phase change process. With the onset of 'convection-only' mode, the interface temperature (i.e. the bottom wall temperature of the recessed cavity) starts to increase sharply as the entire water film is depleted and a subsequent termination of the evaporative cooling process. The additional simulations corresponding to different sets of parameters showed similar repetitive cycles.

The spatial distribution of the water vapor mass fraction and the temperature field at different time instances for the base case is presented in Figure 5.5 and 5.6 respectively. These water vapor mass fraction and temperature profiles correspond to the second cycle (see Figure 5.4) that temporally spans from t = 175 – 350 seconds. The evaporation process occurs till t = 282 seconds which denotes the end point of the coupled convective – evaporative heat transfer process. As shown in Figure 5.5a, during the initiation of the convective-evaporative cycle, water vapor is generated due to evaporation at the interface and then readily gets entrained to the incoming air flow (Figure 5.5b). The maximum evaporation takes place during the early stage of the cycle and then decreases to a quasi-steady rate. In this quasi-steady state, the water vapor mass fraction distribution remains fairly constant in the domain. In the temperature field distribution, one can see that the high temperature near the interface (Figure 5..6a) at the initial stage decreases sharply as the evaporative cooling is initiated. At t = 283 second

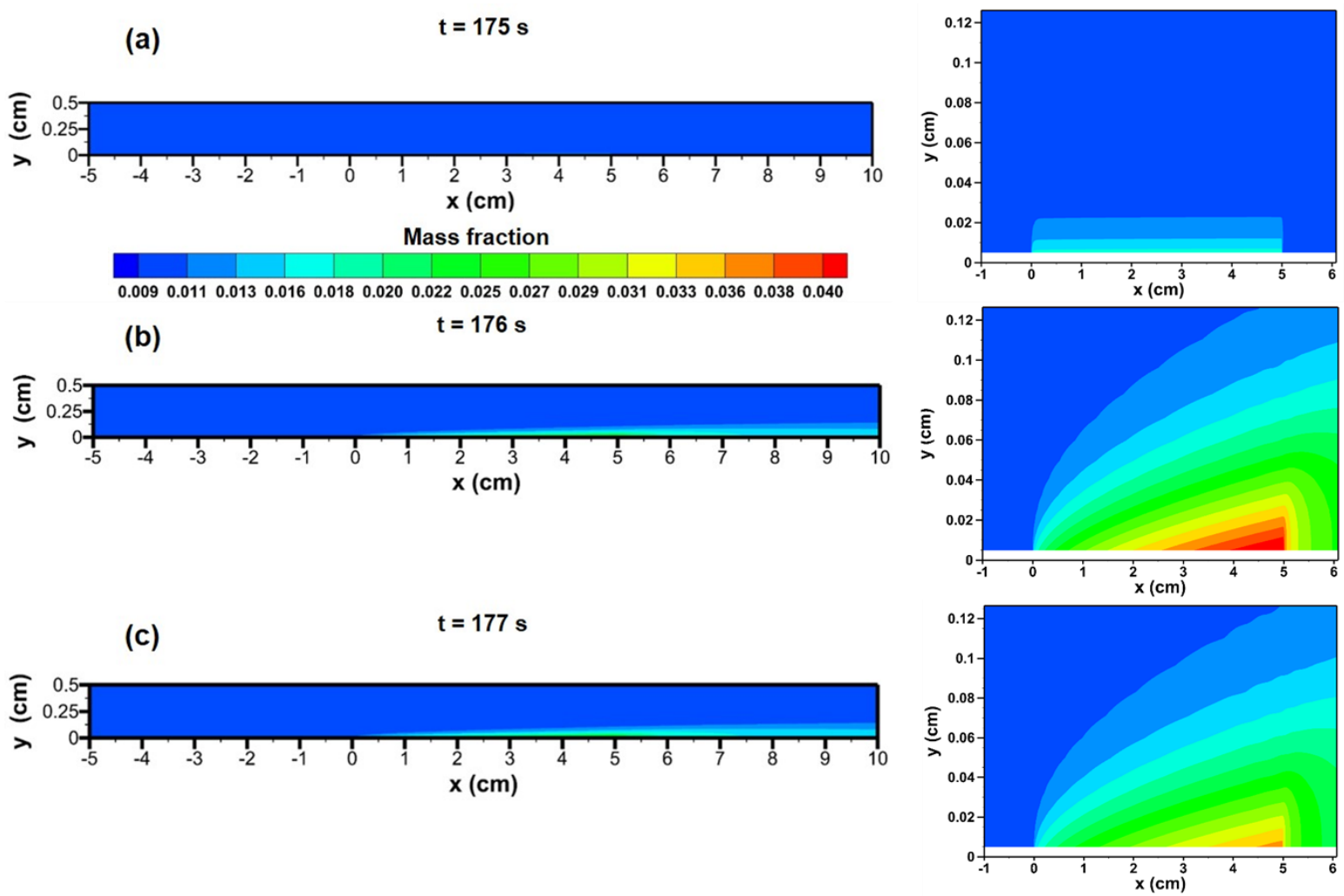
(a)
t = 175 s
y (cm)
x (cm)
Mass fraction
0.009 0.011 0.013 0.016 0.018 0.020 0.022 0.025 0.027 0.029 0.031 0.033 0.036 0.038 0.040
(b)
t = 176 s
y (cm)
x (cm)
(c)
t = 177 s
y (cm)
x (cm)

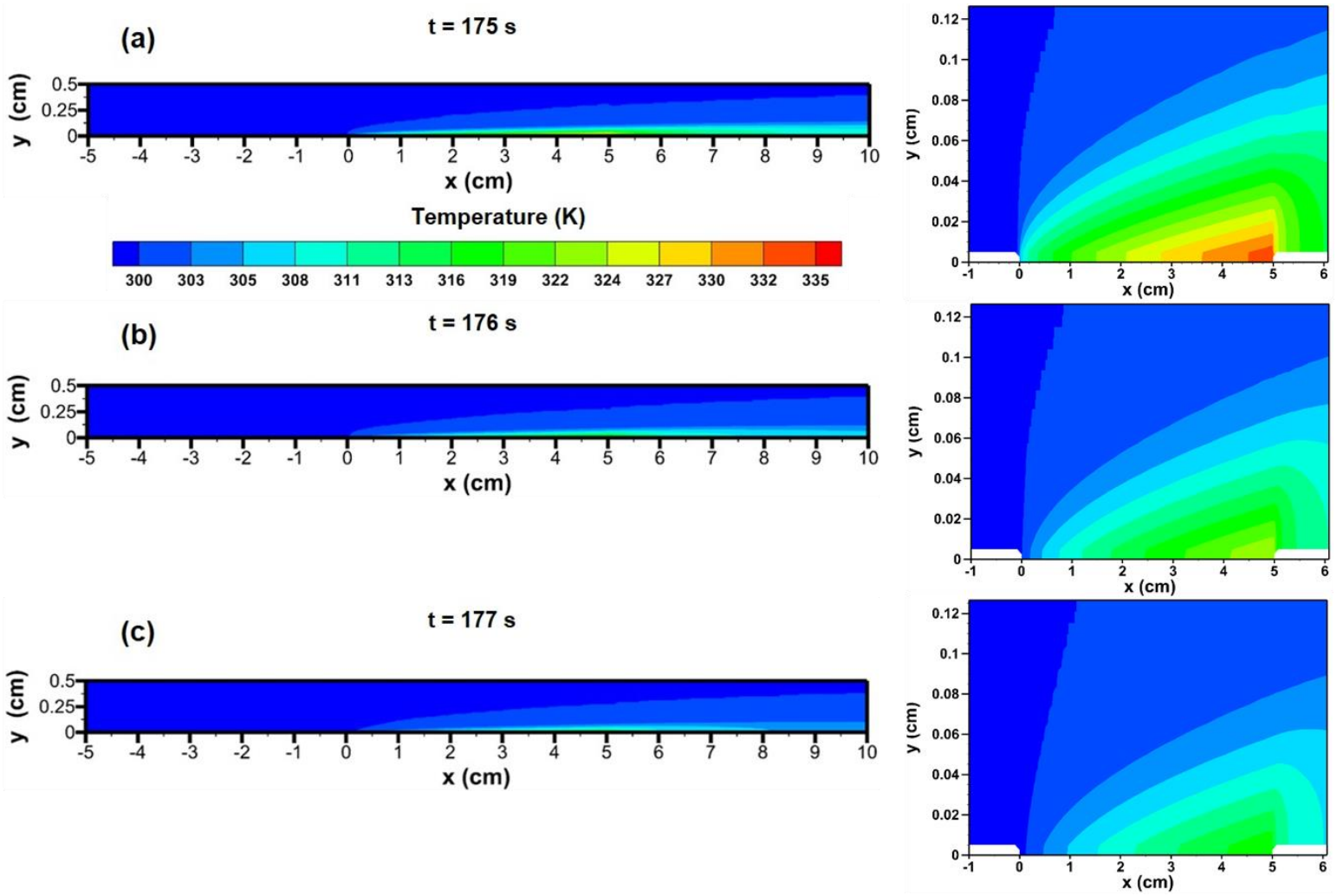

Figure 5.5: Spatial distribution of water vapor mass fraction at different time instances for the base case (U_∞ = 9 m/s/Re = 26007, q_{flux} = 1256 W/m^2, d = 50 μm, σ = 0.0001)

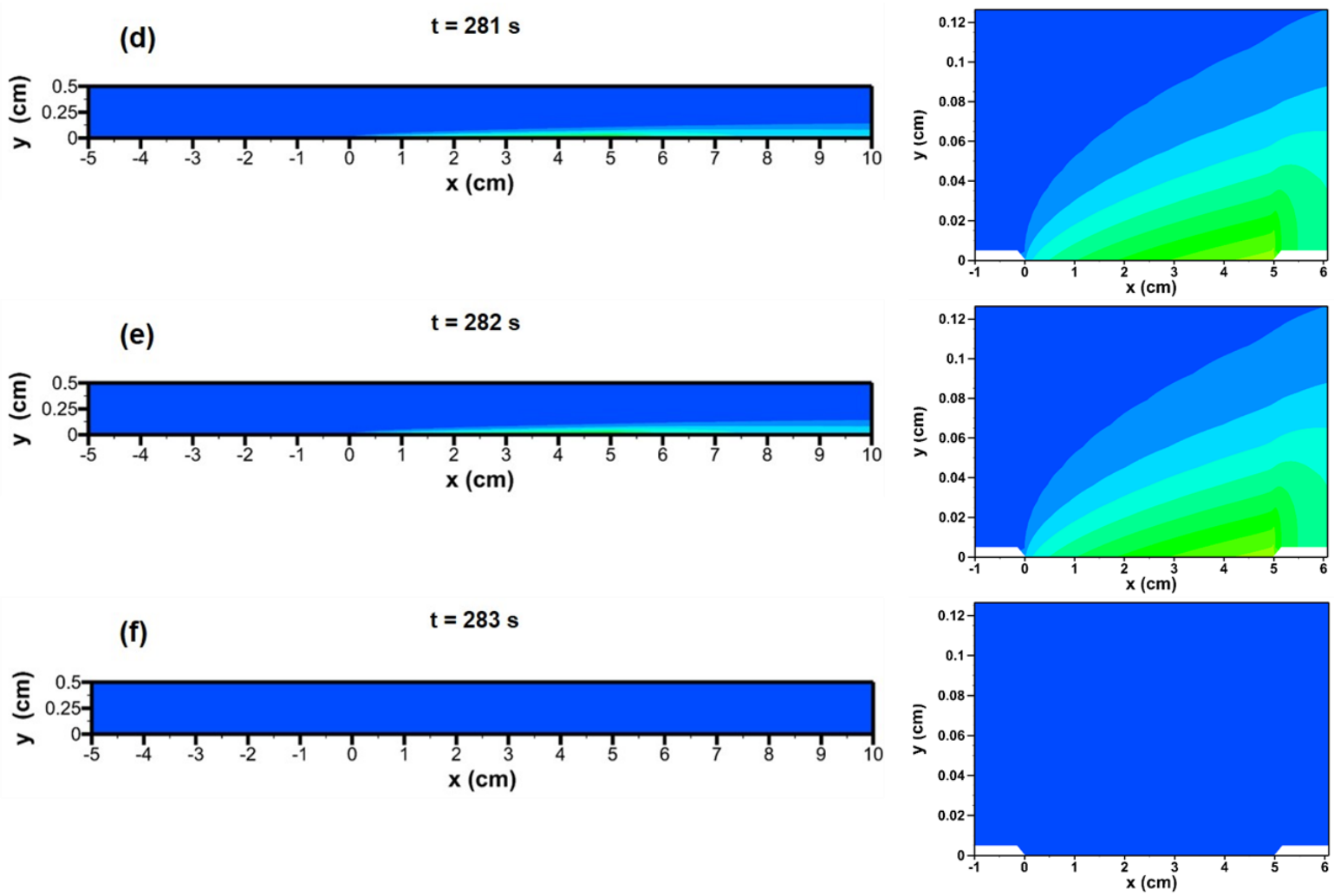
(d)
t = 281 s
y (cm)
x (cm)
(e)
t = 282 s
y (cm)
x (cm)
(f)
t = 283 s
y (cm)
x (cm)

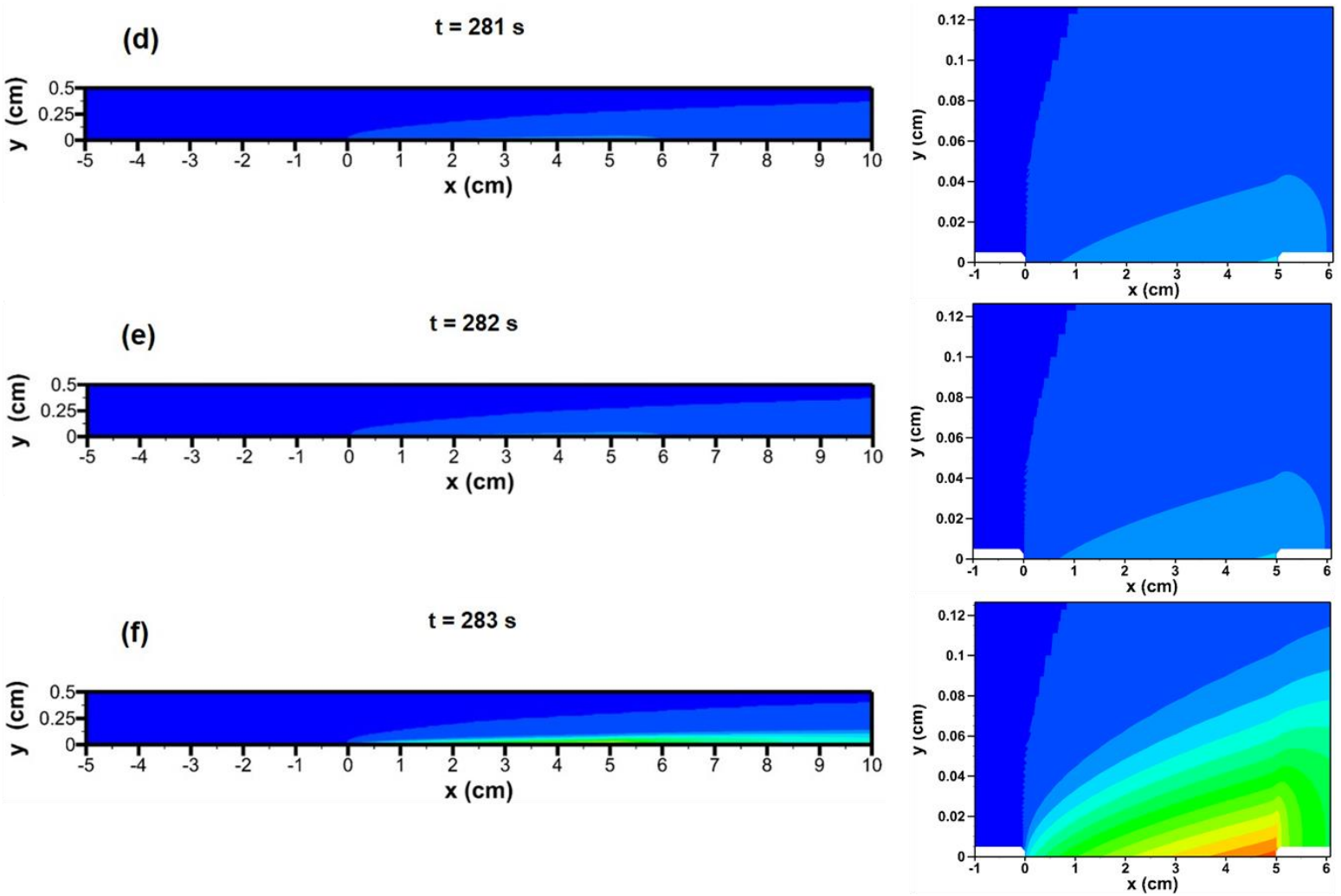

Figure 5.6: Spatial distribution of the temperature field at different time instances for the base case (U_∞ = 9 m/s/Re = 26007, q_{flux} = 1256 W/m^2, d = 50 μm, σ = 0.0001)

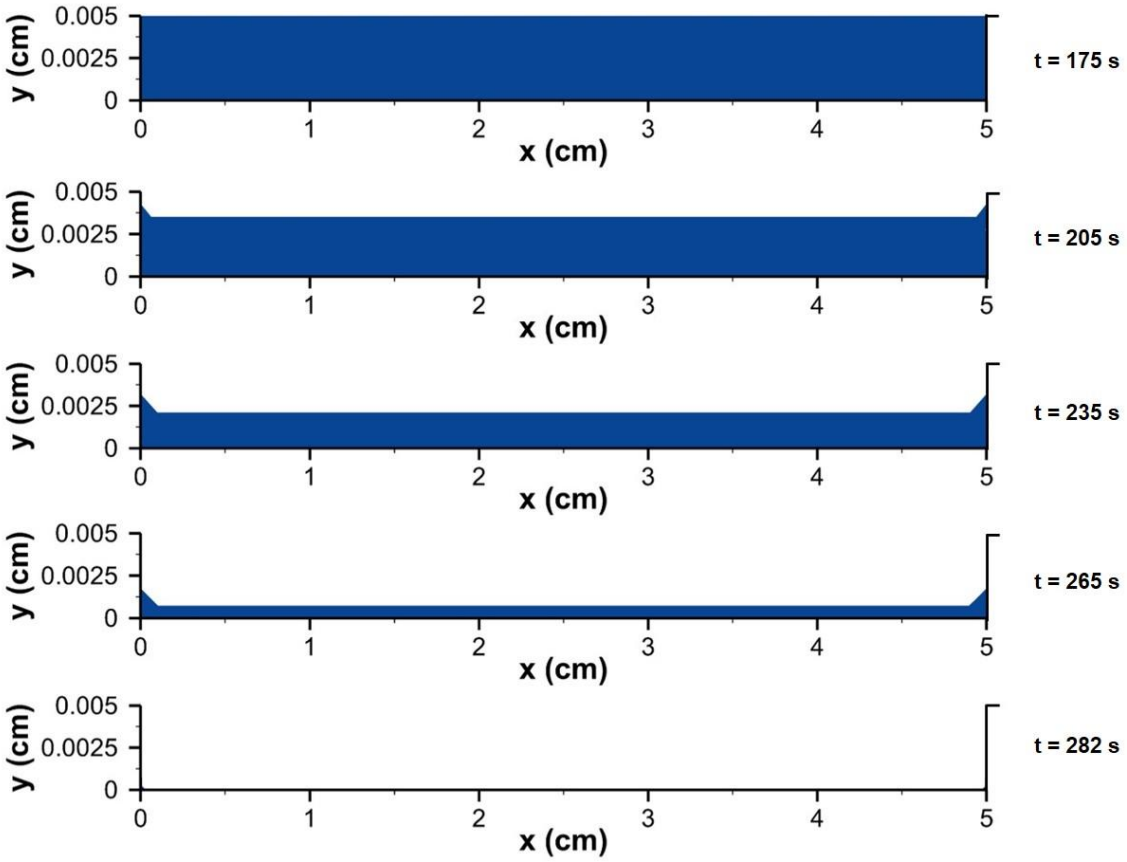

Figure 5.7: Temporal evolution of the liquid film for the base case (U_∞ = 9 m/s/Re = 26007, q_{flux} = 1256 W/m^2, d = 50 μm, σ = 0.0001)

(Figure 5.6f) when the liquid film is completely consumed the temperature distribution reverts back to its high values. It can be generalized that in a single cycle, the large changes in the water vapor mass fraction and temperature distribution takes place during the beginning and end of the evaporation period. The temporal evolution of the liquid film for the same cycle is presented in Figure 5.7, which confirmed that the ALE algorithm was successful in resolving the transient depletion of the liquid film. Only a zoomed inset of the liquid film region is shown here for clarity purpose.

5.3. EFFECT OF REYNOLDS NUMBER AND EVAPORATION FREQUENCY

To investigate the performance of sweating-boosted cooling, an evaporation frequency term, f_{evap} is introduced, $f_{evap} = \frac{t_{SBC}}{t_{SBC} + t_{FCC}}$. In this expression, t_{SBC} and t_{FCC} denote the time associated with sweating-boosted cooling and pure convective cooling respectively. A value of $f_{evap} = 1$ refers to uninterrupted continuous evaporation whereas $f_{evap} = 0$ refers to pure convective mode of operation. The time associated with forced convective cooling t_{FCC}, can be considered to be a control parameter of the system – dictating the time delay between the evaporative and pure convective processes. By controlling the t_{FCC}, one can attain different evaporation frequency (f_{evap}) and alter/achieve heat transfer performance accordingly.

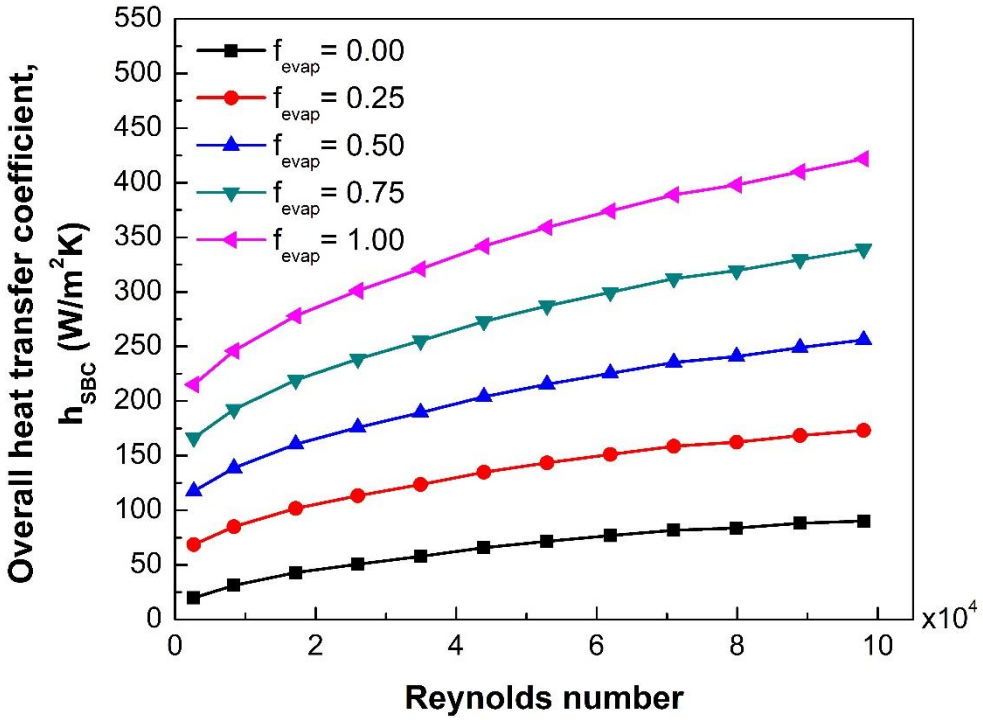

Figure 5.8: Effect of Reynolds number on the overall heat transfer coefficient (q_{flux} = 1256 W/m^2, d = 50 μm, σ = 0.0001)

The effect of Reynolds number on the thermal performance of sweating-boosted cooling for different evaporation frequency (f_{evap}) is summarized in Figure 5.8. The overall heat transfer coefficient represents values that has spatially and temporally averaged over multiple cycles. It is apparent that the combined evaporative and forced convective cooling increases substantially with an increase in the Reynolds number. And, within the entire range of Reynolds number studied, sweating-boosted cooling exhibits significantly higher heat transfer effect than that of pure convection (Figure 5.8, $f_{evap} = 0$).

To compare the cooling effect resulting from phase change and convection, the overall heat transfer coefficient of the coupled convective-evaporative process is normalized to the pure convective condition, $R = \frac{h_{SBC}}{h_{FCC}}$. This normalized overall heat transfer coefficient, R represents the heat transfer enhancement. resulting from the sweating boosted cooling compared to the forced convective cooling. Figure 5.9 depicts the variation of the normalized heat transfer coefficient as a function of Reynolds number. For all the Reynolds number studied with base case condition, this normalized heat transfer coefficient has been found to be greater than unity, ranging from 4 – 11. However, it shows a decreasing trend with the increase of Reynolds number. The sweating boosted cooling is a coupled process where both evaporative and convective cooling simultaneously contribute. In general, the evaporative mass flux increases with local saturation pressure as well as temperature. As a consequence, the evaporative mass flux and the resulting cooling effect is intensified with the increase in local temperature and vice versa. At higher Reynolds, as the convective effect becomes dominant, the gas-

liquid interface temperature reduces which triggers a decrease in the evaporation rate (Figure 5.9). As a result, the evaporative cooling in comparison to the convective cooling effect gradually decreases and eventually plateaus out once a critical Reynolds number is reached (Figure 5.9). In the range of Reynolds number studied for the base case heat flux, film thickness and accommodation coefficient values, the average evaporation flux varies from 0.44 – 0.51 g/m^{2}s which is consistent to both theoretical [47] and experimental measured values [48, 49]. It is noteworthy that, even at the critical Reynolds number (88928 for the base case), the overall heat transfer coefficient of sweating boosted cooling is ~4.5 times of that of pure forced convective cooling (Figure 5.9).

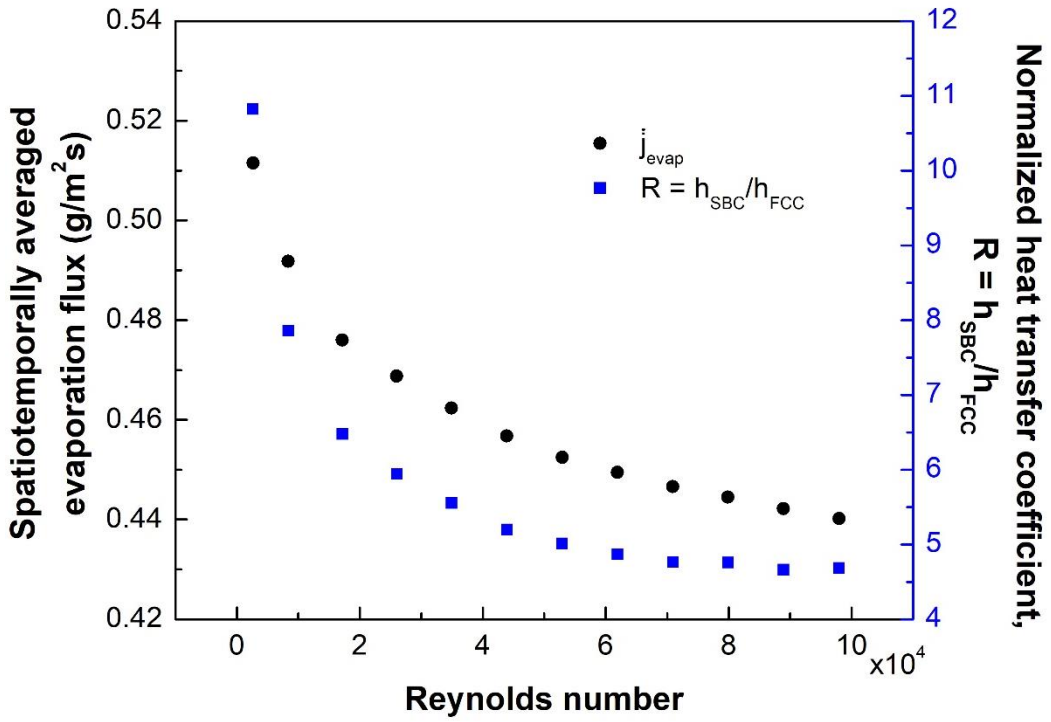

Figure 5.9: Effect of Reynolds number on normalized heat transfer coefficient, $R = h_{SBC} / h_{FCC}$ and average evaporation flux (q_{flux} = 1256 W/m^2, d = 50 μm, σ = 0.0001)

5.4. EFFECT OF FILM THICKNESS

The impact of the liquid film thickness on the performance of sweating-boosted cooling has also been analyzed in this study. Figure 5.10 shows the variation in the overall heat transfer coefficient as a function of film thickness for different Reynolds number condition. It is found that, the overall heat transfer coefficient increases non-linearly with the decrease of film thickness up to a certain limit (~50-200 μm) depending upon Reynolds number. Once this limit is reached, no significant improvement in the overall heat transfer coefficient is noticed with any further decrease of the film thickness.

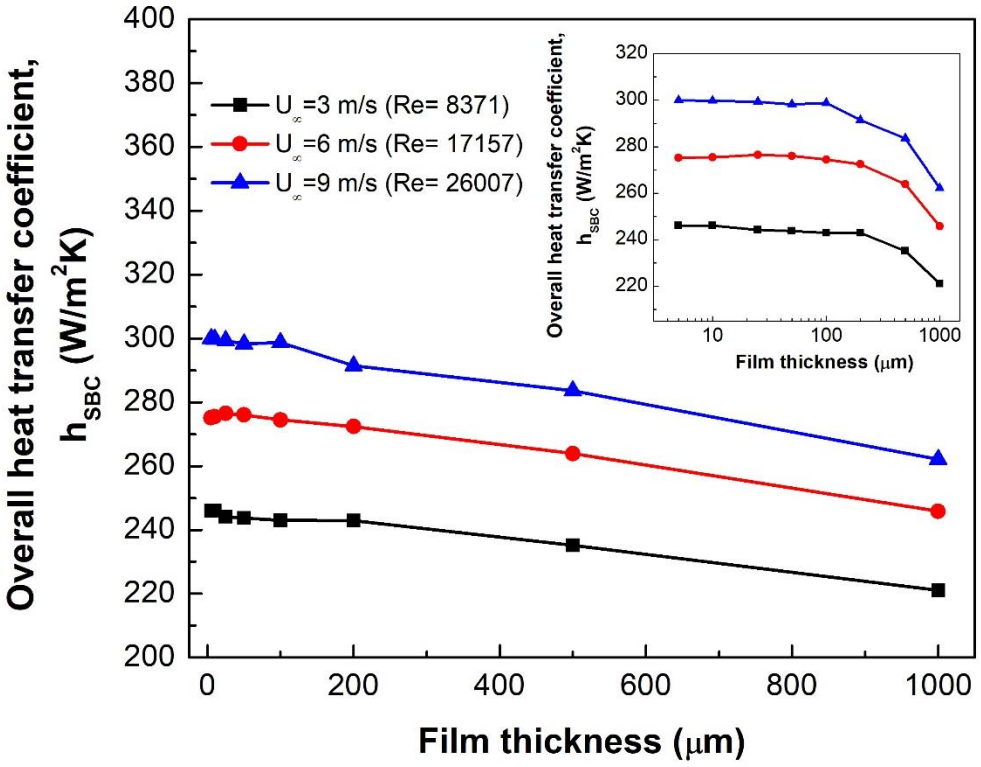

Figure 5.10: Effect of liquid film thickness on the overall heat transfer coefficient for different Reynolds number (q_{flux} = 1256 W/m^2, σ = 0.0001)

Since the prescribed heat flux is provided at the bottom of the liquid phase, thermal resistance across the film defines the overall performance of the system. Thicker film

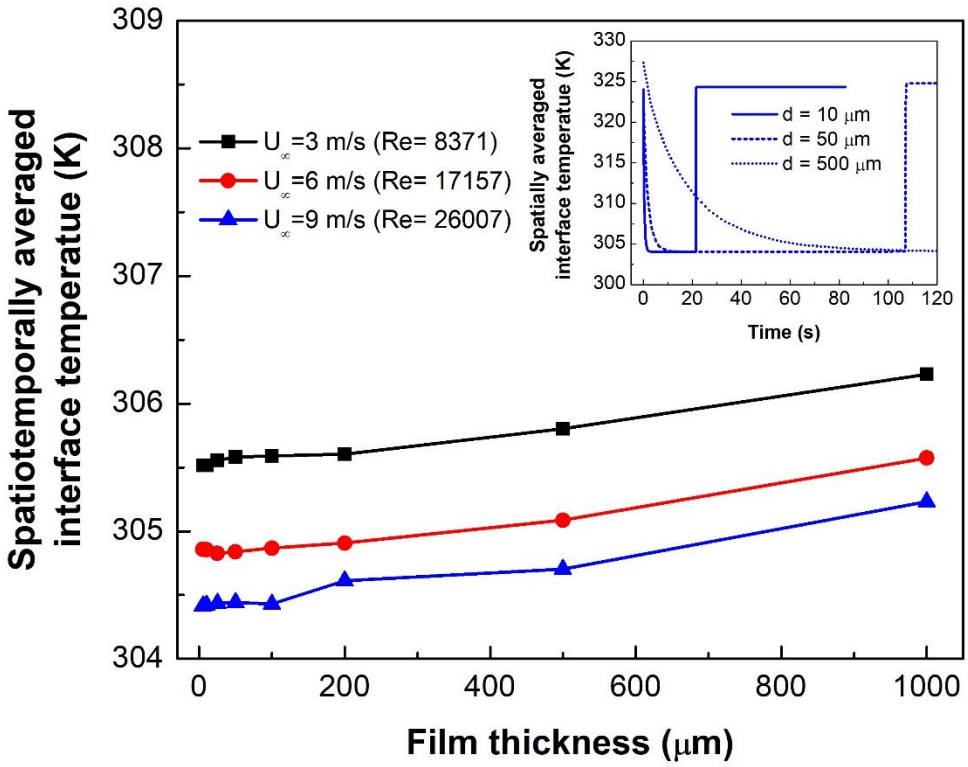

Figure 5.11: Effect of liquid film thickness on the overall heat transfer coefficient for different Reynolds number (q_{flux} = 1256 W/m^2, σ = 0.0001)

results in higher thermal inertia which leads to a suppressed thermal performance. To investigate the role of film thickness in augmenting thermal inertia, spatiotemporally averaged interface temperature has been presented for different film thicknesses in Figure 5.11. It is evident that beyond the critical film thickness value, the thermal inertia of the system becomes dominant and the interface temperature shows an increasing trend with film thickness; an evident attenuation of the cooling process. The inset graph of Figure 5.11 shows the temporal evolution of the spatially averaged interface temperature for three different film thickness for a Reynolds number of 26007. For a film thickness of 10 μm, the convective-evaporative process decreases the temperature almost instantly and the film is completely evaporated within ~20s. Whereas, during this time period, the 500

μm liquid film is yet to respond to the system dynamics to reach a quasi-steady interface temperature at which evaporation takes place. This delayed temporal response of the thicker films results in a decrease in the overall heat transfer coefficient.

5.5. IMPACT OF ACCOMMOCATION COEFFICIENT IN HERTZ-KNUDSEN EXPRESSION ON OVERALL HEAT TRANSFER PERFORMANCE AND EXPERIMENTAL VALIDATION

Even though the Hertz-Knudsen relation has been extensively employed in modeling evaporation process, it has often been found that evaporation flux predicted by the Hertz-Knudsen relationship varies significantly with the experimental results. One of the major uncertainties in the Hertz-Knudsen relationship is rooted to the evaporation and condensation coefficients [37, 38, 40]. In many prior studies [39, 40, 48, 50] both the coefficients are assumed to be equal and thereby lumped into a single accommodation coefficient (σ). Numerous experiments [48, 51-54] have shown a large spread/scatter in the accommodation coefficient value – varying by four orders of magnitude at times. Davis et al. [53] used the Hertz-Knudsen relationship to determine the values of σ by investigating evaporation process of water and isopropanol. Surprisingly, they found σ to be greater than unity. Marek and Straub [38] raised concerns on the common assumption that the HK coefficients are constant properties of a substance. On the contrary, their study concluded that the values of the coefficients vary with different parameters, among them impurities and surface condition (temperature and pressure) are the most dominant factors. Their evaluation observed a decrease in both coefficients as the temperature increases. Very recently, Persad and Ward [37] provided a thorough review on this topic and conducted an extensive series of experiments with a goal to identify the possible

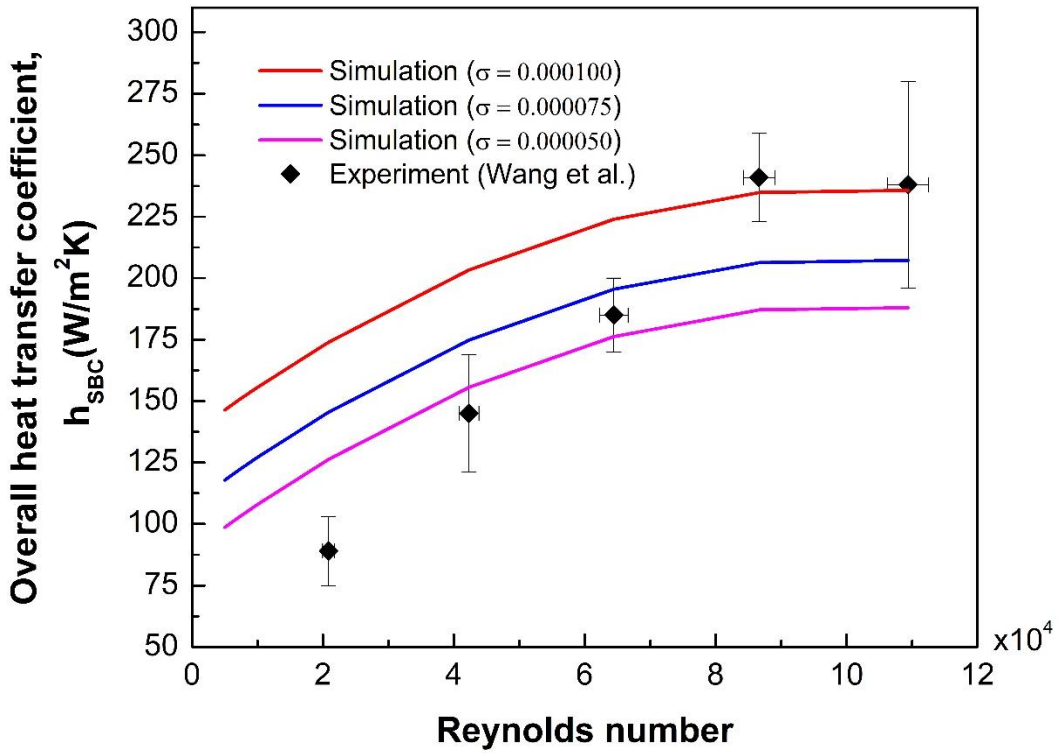

Figure 5.12: Impact of accommodation coefficient values on the predicted overall heat transfer coefficient for different Reynold's number conditions (q_{flux} = 1256 W/m^2, d = 50 μm). The numerical predictions are also compared against the experimental measurements of Wang et al. [21]

reason for the large scatter in the accommodation coefficient values. They identified interfacial curvature, molecular structure of the fluid, capillary waves, temperature, Reynolds number to be the source of the variation in the accommodation coefficient values. Here we conducted a sensitivity analysis of the predictions on the chosen accommodation coefficient values. An estimation of the accommodation coefficient on the basis of kinetic theory is beyond the scope of this current work. Figure 5.12 summarizes the influence of the accommodation coefficient values on the predicted overall heat transfer coefficient The predictions are further compared against the experimental measurements of Wang et al. [21, 22] It is apparent that an increase in the accommodation coefficient increases the overall heat transfer coefficient. The model is

able to predict the general trend in the heat transfer coefficient variation as a function of the Reynold's number. The spread in the numerical predictions resulting from the accommodation coefficient values overlaps with the experimental measurements.

5.6. ANLYSIS ON WATER CONSUMPTION AND FOOTPRINT REDUCTION

The sweating-boosted cooling (SBC) method has been proposed with a view to finding a trade-off between air-cooled and water-cooled condenser. In order to asses this, we have compared the global features i.e., equivalent heat exchanger area and water consumption of SBC with pure water-cooled system (h = 2000 W/m^{2}K [46]) and air-cooled system (h = 90 W/m^{2}K [46]). Figure 5.13 shows the comparison between the equivalent heat exchanger area requirement and water consumption of conventional cooling methods and the proposed hybrid mode heat transfer for a fixed temperature gradient. The water consumption of sweating-boosted cooling is reduced to 21% compared to a fully water-cooled system which is eventually achieved by compromising the heat transfer coefficient. However, to find a trade-off between area footprint in air-cooling system and water consumption in water-cooling system, proposed hybrid cooling method shows significant improvement. Area requirement for water-cooled system has been found to be minimum (~36 m^2/MW) due to the very high heat transfer coefficient associated with it and vice versa for the air-cooled system (~815 m^2/MW). With the hybrid cooling method, the area requirement reduces drastically while still maintaining a higher heat transfer coefficient compared to that of the dry cooling. Sweating boosted cooling with water replenishing frequency of 8.92 mHz provides a ~78% size reduction compared to pure air-cooling method while delivering an improvement of heat transfer coefficient (422 W/m^{2}K) by a factor a of ~5.

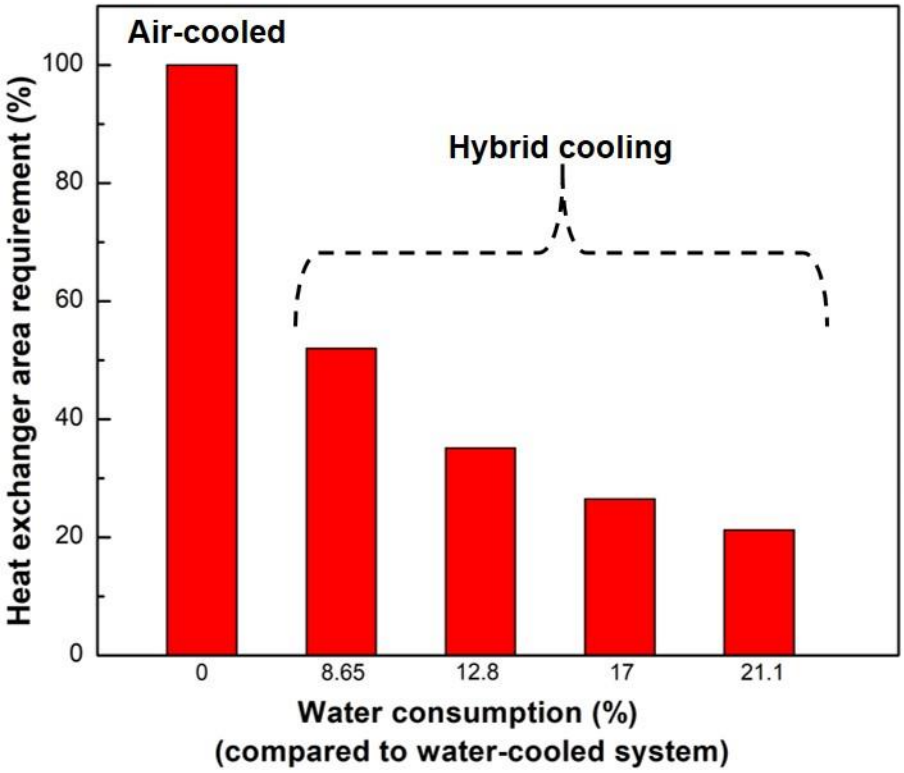

Figure 5.13: Heat exchanger area as a function of water consumption

5.7. EFFECT OF SURFACE STRUCTURE MODIFICATION ON HYBRID COOLING SYSTEM

As an extension of the flat liquid film evaporation under convective loading, simulations have been conducted for modified surface textures. From the previous analysis, it is evident that the conduction resistance across the liquid film plays a vital role in determining overall cooling performance. Hereby, we have introduced circular grooves on the bottom surface of the liquid film with a view to suppressing the thermal resistance across the liquid film. Parametric studies were conducted by varying the diameter of the circular grooves. Schematic representation of the three different configurations of the modified structures is presented in Figure 5.14. The details of the configurations for the modified surface structures are listed in Table 5.1.

Table 5-1: Specifications of the modified structure arrangement

Configuration	Radius of circular groove (μm)	Number of grooves
A	225	24
B	450	24
C	1000	12

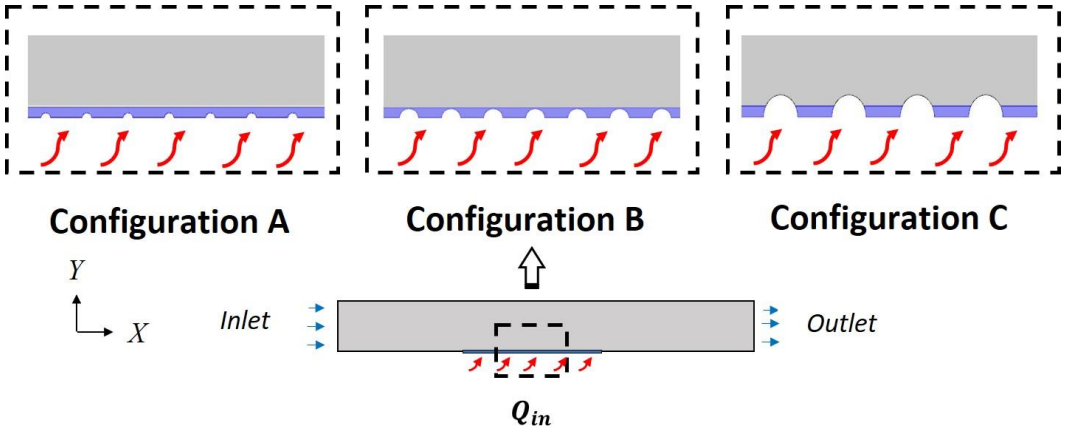

Figure 5.14: Schematic diagram of the modified bottom surface of the recessed region

To analyze the effect of surface modification, the thermal resistance of a modified structure is calculated, then normalized with the flat film configuration. The normalized thermal resistance, R_{norm} has been calculated as follows:

$$R_{norm} = \frac{\left[\left(T_b - T_\infty\right)_{modified}\right]/Q_{in}}{\left[\left(T_b - T_\infty\right)_{flat\ film}\right]/Q_{in}} = \frac{\left(\Delta T\right)_{modified}}{\left(\Delta T\right)_{flat\ film}} \tag{13}$$

where, T_b is the steady state bottom surface temperature, T_∞ is the inlet temperature and Q_{in} is the heat input at bottom surface. The normalized thermal resistances for the different configuration studies are shown in Figure 5.15. For all cases, the normalized thermal coefficient has been found to be less than unity, providing evidence of enhanced

cooling compared to the simple flat film configuration. configuration A predicts a very small reduction

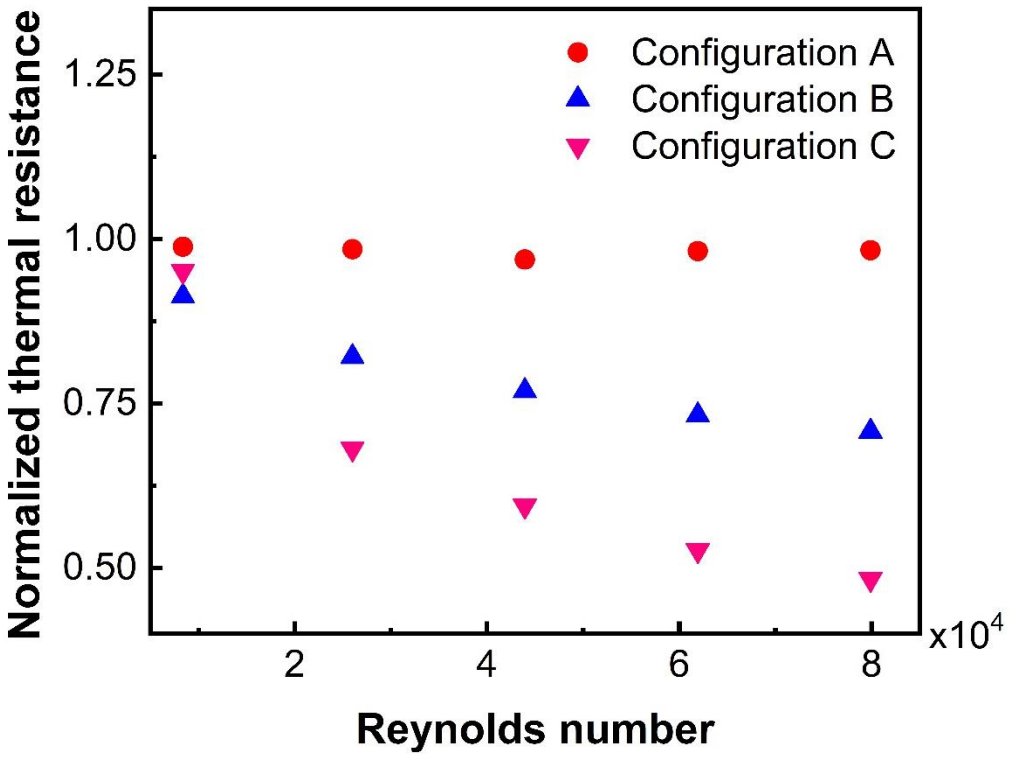

Figure 5.15: Thermal resistance of modified structures normalized by similar flat film configuration

in thermal resistance (~2%), whereas, configuration C has been found to reduce the thermal resistance by almost 50% at a Reynolds number of ~80000. The advantage of modified surface structure over a flat film configuration has been schematically presented in Figure 5.16. With the flat film configuration, the thermal resistance is higher because heat is traveling in a unidirectional way. On the contrary, with the introduction of circular grooves energy is supplied to the evaporating liquid from multiple directions, resulting in a reduction of conductive loss across the liquid film. In the case of configuration C, the grooves are further elevated across the air domain to promote mixing, ultimately leading to intensified evaporation and a significant reduction of thermal resistance.

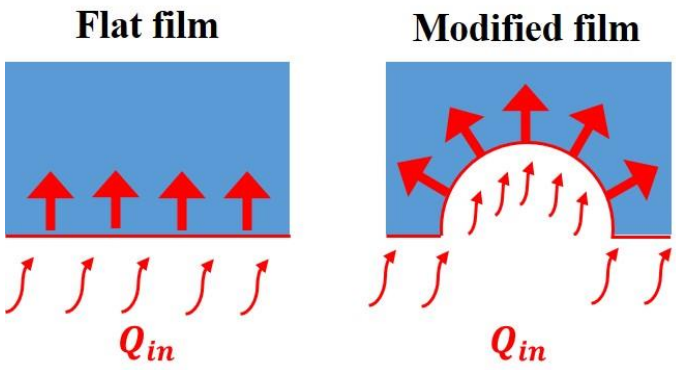

Figure 5.16: Schematic representation of direction of conduction heat transfer through liquid film for flat and modified bottom surface structure

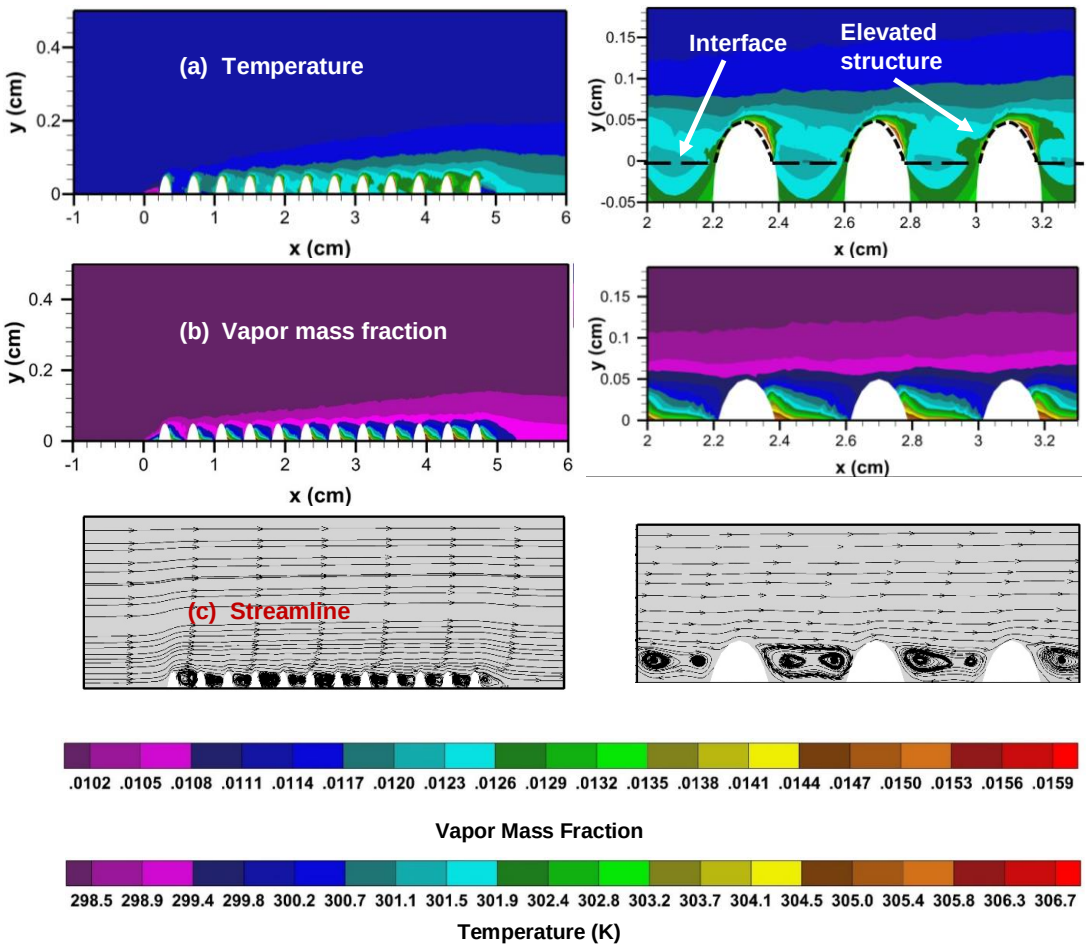

Figure 5.17: Distribution of (a) temperature, (b) vapor mass fraction and (c) streamline pattern for design C. The distribution is magnified over fewer elevated structure on right hand side column for clarity purpose

Since Configuration C provides the highest reduction in thermal resistance and greatest enhancement in evaporation flux in this study, spatial distribution of temperature and vapor mass fraction for configuration C has been investigated here. Figure 5.17 depicts the contour plots of temperature and vapor mass fraction distribution along with streamline pattern for configuration C. It is evident from the streamline patterns that configuration C promotes mixing owing to having elevated structure inserted into the gas domain. A region of hotter temperature zone (~306 K) is observed at the descending side of the elevated structure (Figure 5.17a) due to the existence of recirculation around that area (Figure 5.17c). However, followed by the hotter zone, a colder temperature region (~301 K) is observed along the interface where the evaporation is taking place and cooling effect is maximum due to high phase change energy consumption. Even though, uniform evaporation mass flux has been prescribed at the interface, highest vapor mass fraction is observed at the trailing end of the elevated structure. Vapor is forming at the interface and accumulates at the trailing zone of the interface due to the recirculation and then diffused to the gas domain and eventually carried away by the incoming air flow.

CHAPTER 6

CONCLUSION

6.1. MAJOR CONTRIBUTIONS

A fully coupled model of sweating boosted cooling method has been presented where both convection and evaporation contribute to the overall heat transfer process. Mass, momentum, energy and species transport were solved along with a moving mesh technique to capture the recession of liquid film that is being evaporated. The Hertz-Knudsen relation has been applied to predict the evaporation flux at liquid-gas interface. Simulations have been conducted within a wide range of Reynolds number for different liquid film thicknesses. Significant improvement in the overall heat transfer coefficient is observed in the hybrid cooling mode of operation. For all the cases studied, the normalized heat transfer coefficient (ratio of overall heat transfer coefficient of sweating boosted cooling to that of pure convective cooling) has been found to be greater than unity but decreases as the flow Reynolds number is increased. A critical Reynolds number has been identified beyond which the performance of sweating-boosted cooling reaches a plateau and no further enhancement of the heat transfer coefficient resulting from the phase change process is observed. Even at the critical Reynolds number, in comparison to the pure convection condition, the sweating-boosted cooling increases the overall heat transfer coefficient by a factor of 4 – 5.

Film thickness has been found to be one of the key parameters in determining the overall thermal performance. At larger film thickness the predictions show that the thermal inertia becomes dominant and can suppress the overall thermal performance. The numerical results are in good agreement in capturing the general trend of experimental observations. The maximum heat transfer coefficient achieved by this proposed model was 422 W/m^2K with a ~78% reduction of area footprint compared to a complete dry cooling method.

Simulations have been conducted with modified surface structure with a view to minimizing the conductive loss across the liquid film. Circular grooves have been introduced on the bottom surface so that energy can be provided to the evaporating liquid from multidirectional way. Preliminary studies predict that modified structures exhibit significant reduction in overall thermal resistance. With the arrays of circular grooves of 1000 micron, thermal resistance has been found to be reduced by 50% compared to similar flat film configuration.

6.2. FUTURE RECOMMENDATION

The following recommendations are made for future studies:

- Momentum conservation in liquid phase. In this study, only conduction heat transfer has been considered through the liquid film. Therefore, the momentum transform across the liquid film has not been resolved. Due to the high convective flow of air, there should be some rippling effect on water surface which will eventually affect the overall heat transfer process. However, solving momentum transport in liquid phase along with current arrangement may be computationally expensive. Thus, if the rippling effect is dominating enough to make significant

changes in the overall heat transfer coefficient, it may be necessary to solve the momentum transport in liquid phase. Author recommends addressing this concern as an extension of current numerical model.

- Heat transfer through porous media. One of the major bottlenecks in the evaporation assisted convective cooling described here is the low thermal conductivity of the liquid. Evaporation occurs on the surface and the system response time is dictated by the thermal resistance across the liquid film. The cooling performance can be further boosted up if the conductive loss across the liquid film can be minimized. This challenge can be mitigated by introducing a porous media with a high conductivity. Furthermore, porous media also acts as a liquid storage in microscopic level. Hence, current models can be further extended for heat transfer through porous media which can act as a storage for the evaporative liquid.
- Incorporation of ‘temperature jump’ at the interface. Most of the works in this field of study are based on the simplified version of HK relation that ignores the temperature discontinuity along the liquid-gas interface. This is because it requires a heavily scrutinized numerical model that is beyond the continuum regime of fluid flow. Author recommends to address this concern as an advanced extension of this work.
- Robust analysis on surface structure modification. This thesis work describes the preliminary findings of surface modification on the heat transfer enhancement in hybrid cooling system. Numerical analyses qualitatively predict significant reduction in thermal resistance and enhanced cooling with modified structures.

However, comprehensive studies are required to find further details for the performance of proposed hybrid cooling system in this regard.

REFERENCES

[1] N.L.B. Joan F. Kenny, Susan S. Hutson, Kristin S. Linsey, John K. Lovelace, Molly A. Maupin, Estimated use of water in the United States in 2005, 2009.

[2] C.A. Dieter, M.A. Maupin, R.R. Caldwell, M.A. Harris, T.I. Ivahnenko, J.K. Lovelace, N.L. Barber, K.S. Linsey, Estimated use of water in the United States in 2015, 1441, Reston, VA, 2018.

[3] M.A.H. Timothy H. Diehl, Jennifer C. Murphy, Susan S. Hutson, and David E. Ladd, Methods for Estimating Water Consumption for Thermoelectric Power Plants in the United States, in, U.S. Geological Survey Scientific Investigations Report 2013–5188, 2013.

[4] C.o.E. Quality, Implementing Instructions: Federal Agency,Implementation of Water Efficiency and, Management Provisions of EO 13514, in, 2013.

[5] J.G. Bustamante, A.S. Rattner, S. Garimella, Achieving near-water-cooled power plant performance with air-cooled condensers, Applied Thermal Engineering, 105 (2016) 362-371.

[6] A. Tikadar, U. Najeeb, T.C. Paul, S.K. Oudah, A.S. Salman, A.M. Abir, L.A. Carrilho, J.A. Khan, Numerical investigation of heat transfer and pressure drop in nuclear fuel rod with three-dimensional surface roughness, International Journal of Heat and Mass Transfer, 126 (2018) 493-507.

[7] S.E.B. Maïga, S.J. Palm, C.T. Nguyen, G. Roy, N. Galanis, Heat transfer enhancement by using nanofluids in forced convection flows, International Journal of Heat and Fluid Flow, 26(4) (2005) 530-546.

[8] R. Kabir, K. Kaddoura, F.P. McCluskey, J.P. Kizito, Investigation of a Cooling System for A Hybrid Airplane, 2018 AIAA/IEEE Electric Aircraft Technologies Symposium (EATS), 2018, pp. 1-18.

[9] J. Xu, T.S. Fisher, Enhancement of thermal interface materials with carbon nanotube arrays, International Journal of Heat and Mass Transfer, 49(9) (2006) 1658-1666.

[10] L. Godson, B. Raja, D. Mohan Lal, S. Wongwises, Enhancement of heat transfer using nanofluids—An overview, Renewable and Sustainable Energy Reviews, 14(2) (2010) 629-641.

[11] X.-Q. Wang, A.S. Mujumdar, Heat transfer characteristics of nanofluids: a review, International Journal of Thermal Sciences, 46(1) (2007) 1-19.

[12] D. Wen, Y. Ding, Formulation of nanofluids for natural convective heat transfer applications, International Journal of Heat and Fluid Flow, 26(6) (2005) 855-864.

[13] P.-X. Jiang, G.-S. Si, M. Li, Z.-P. Ren, Experimental and numerical investigation of forced convection heat transfer of air in non-sintered porous media, Experimental Thermal and Fluid Science, 28(6) (2004) 545-555.

[14] A.A. Mohamad, Heat transfer enhancements in heat exchangers fitted with porous media Part I: constant wall temperature, International Journal of Thermal Sciences, 42(4) (2003) 385-395.

[15] R. Boubaker, S. Harmand, V. Platel, Experimental study of the liquid/vapor phase change in a porous media of two-phase heat transfer devices, Applied Thermal Engineering, 143 (2018) 275-282.

[16] B.X. Wang, X.F. Peng, Experimental investigation on liquid forced-convection heat transfer through microchannels, International Journal of Heat and Mass Transfer, 37 (1994) 73-82.

[17] G.L. Morini, Single-phase convective heat transfer in microchannels: a review of experimental results, International Journal of Thermal Sciences, 43(7) (2004) 631-651.

[18] A.K. Sadaghiani, N.S. Saadi, S.S. Parapari, T. Karabacak, M. Keskinoz, A. Koşar, Boiling heat transfer performance enhancement using micro and nano structured surfaces for high heat flux electronics cooling systems, Applied Thermal Engineering, 127 (2017) 484-498.

[19] A.S. Salman, N.M. Abdulrazzaq, S.K. Oudah, A. Tikadar, N. Anumbe, T.C. Paul, J.A. Khan, Experimental investigation of the impact of geometrical surface modification on spray cooling heat transfer performance in the non-boiling regime, International Journal of Heat and Mass Transfer, 133 (2019) 330-340.

[20] N.A. Nabeel M. Abdulrazzaq, Jamil Khan, Experimental investigation of the performance of refrigerant R134A working in a spray cooling, in: 3rd Thermal and Fluids Engineering Conference, Fort Lauderdale, FL, USA, 2018.

[21] P. Wang, R. Dawas, M. Alwazzan, M. Stefik, J. Khan, C. Li, Sweating-Boosted Air Cooling With Water Dripping, ASME 2016 Summer Heat Transfer Conference, Bellevue, WA, USA, 2016.

[22] P. Wang, R. Dawas, M. Alwazzan, W. Chang, J. Khan, C. Li, Sweating-boosted air cooling using nanoscale CuO wick structures, International Journal of Heat and Mass Transfer, 111 (2017) 817-826.

[23] S. Saha, R. Mahamud, J. Khan, T. Farouk, Simulation of Sweating/Evaporation Boosted Convective Heat Transfer Under Laminar Flow Condition, ASME 2017 Summer Heat Transfer Conference, Bellevue, USA, 2017.

[24] Y. Wei-Mon, Effects of film evaporation on laminar mixed convection heat and mass transfer in a vertical channel, International Journal of Heat and Mass Transfer, 35(12) (1992) 3419-3429.

[25] W.-M. Yan, Effects of film vaporization on turbulent mixed convection heat and mass transfer in a vertical channel, International Journal of Heat and Mass Transfer, 38(4) (1995) 713-722.

[26] A. Bejan, K.R. Khair, Heat and mass transfer by natural convection in a porous medium, International Journal of Heat and Mass Transfer, 28(5) (1985) 909-918.

[27] N. Boukadida, S. Ben Nasrallah, Mass and heat transfer during water evaporation in laminar flow inside a rectangular channel—validity of heat and mass transfer analogy, International Journal of Thermal Sciences, 40(1) (2001) 67-81.

[28] V.V. Vyazovov, A theory of absorption of slightly soluble gases by liquid films, J. Tech. Phys.(USSR), 10 (1940) 1519-1532.

[29] W.E. Olbrich, J.D. Wild, Diffusion from the free surface into a liquid film in laminar flow over defined shapes, Chemical Engineering Science, 24(1) (1969) 25-32.

[30] G. Grossman, Simultaneous heat and mass transfer in film absorption under laminar flow, International Journal of Heat and Mass Transfer, 26(3) (1983) 357-371.

[31] S.-M. Yih, R.C. Seagrave, Mass transfer in laminar falling liquid films with accompanying heat transfer and interfacial shear, International Journal of Heat and Mass Transfer, 23(6) (1980) 749-758.

[32] W.M. Yan, Y.L. Tsay, T.F. Lin, Simultaneous heat and mass transfer in laminar mixed convection flows between vertical parallel plates with asymmetric heating, International Journal of Heat and Fluid Flow, 10(3) (1989) 262-269.

[33] S. Whitaker, Simultaneous Heat, Mass, and Momentum Transfer in Porous Media: A Theory of Drying, in: P.H. James, F.I. Thomas (Eds.) Advances in Heat Transfer, Elsevier, 1977, pp. 119-203.

[34] L.C. Chow, J.N. Chung, Evaporation of water into a laminar stream of air and superheated steam, International Journal of Heat and Mass Transfer, 26(3) (1983) 373-380.

[35] A.S. Cherif, M.A. Kassim, B. Benhamou, S. Harmand, J.P. Corriou, S. Ben Jabrallah, Experimental and numerical study of mixed convection heat and mass transfer in a vertical channel with film evaporation, International Journal of Thermal Sciences, 50(6) (2011) 942-953.

[36] M. Knudsen, Kinetic Theory of Gases, 3rd ed., London Methuen, London, 1950.

[37] A.H. Persad, C.A. Ward, Expressions for the evaporation and condensation coefficients in the Hertz-Knudsen relation, Chemical Reviews, 116(14) (2016) 7727-7767.

[38] R. Marek, J. Straub, Analysis of the evaporation coefficient and the condensation coefficient of water, International Journal of Heat and Mass Transfer, 44(1) (2001) 39-53.

[39] P. Davidovits, D.R. Worsnop, L.R. Williams, C.E. Kolb, M. Gershenzon, Comment on “Mass accommodation coefficient of water: Molecular dynamics simulation and revised analysis of droplet train/flow reactor experiment”, The Journal of Physical Chemistry B, 109(30) (2005) 14742-14746.

[40] R. Hołyst, M. Litniewski, D. Jakubczyk, K. Kolwas, M. Kolwas, K. Kowalski, S. Migacz, S. Palesa, M. Zientara, Evaporation of freely suspended single droplets: experimental, theoretical and computational simulations, Reports on Progress in Physics, 76(3) (2013) 034601.

[41] M. Mozurkewich, Aerosol growth and the condensation coefficient for water: A review, Aerosol science and technology, 5(2) (1986) 223-236.

[42] G.W. Thomson, The Antoine equation for vapor-pressure data, Chemical Reviews, 38(1) (1946) 1-39.

[43] M. Souli, J.P. Zolesio, Arbitrary Lagrangian–Eulerian and free surface methods in fluid mechanics, Computer Methods in Applied Mechanics and Engineering, 191(3–5) (2001) 451-466.

[44] I. COMSOL, COMSOL Multiphysics® 4.4, in, 2013.

[45] P.R. Amestoy, I.S. Duff, J.Y. L'Excellent, Multifrontal parallel distributed symmetric and unsymmetric solvers, Computer Methods in Applied Mechanics and Engineering, 184(2–4) (2000) 501-520.

[46] D.P.D. Frank P. Incropera, Theodore L. Bergman , Adrienne S. Lavine Fundamentals of Heat and Mass Transfer, 7th ed., John Wiley & Sons, 2011.

[47] P.N. Shankar, F.E. Marble, Kinetic theory of transient condensation and evaporation at a plane surface, The physics of fluids, 14(3) (1971) 510-516.

[48] V.K. Badam, V. Kumar, F. Durst, K. Danov, Experimental and theoretical investigations on interfacial temperature jumps during evaporation, Experimental Thermal and Fluid Science, 32(1) (2007) 276-292.

[49] G. Fang, C.A. Ward, Temperature measured close to the interface of an evaporating liquid, Physical Review E, 59(1) (1999) 417.

[50] G.T. Barnes, The effects of monolayers on the evaporation of liquids, Advances in Colloid and Interface Science, 25 (1986) 89-200.

[51] N. Fukuta, M.N. Myers, Simultaneous Measurement of Condensation and Thermal Accommodation Coefficients for Cloud Droplet Growth in Due Consideration of a New Moving Surface-Boundary Effect, Journal of the Atmospheric Sciences, 64(3) (2007) 955-968.

[52] J.B. Young, The condensation and evaporation of liquid droplets at arbitrary Knudsen number in the presence of an inert gas, International Journal of Heat and Mass Transfer, 36(11) (1993) 2941-2956.

[53] E.J. Davis, A history and state-of-the-art of accommodation coefficients, Atmospheric Research, 82(3) (2006) 561-578.

[54] P.M. Winkler, A. Vrtala, P.E. Wagner, M. Kulmala, K.E.J. Lehtinen, T. Vesala, Mass and Thermal Accommodation during Gas-Liquid Condensation of Water, Physical Review Letters, 93(7) (2004) 075701.